Synthesis and characterization of adsorbents based on RGO for removing heavy metal ions via cooperation mechanism

by

Roshanak Miraftab

Bachelor of Science, Amirkabir University of Technology, 2013

A Thesis Submitted in Partial Fulfillment
of the Requirements for the Degree of

Master of Science

in the Graduate Academic Unit of Chemical Engineering

Supervisor: Huining Xiao, Ph.D., Chemical Engineering

Examining Board: Brian Lowry, Ph.D., Chemical Engineering
Zhibin (Ben) He, Ph.D., Chemical Engineering
Meng Gong, Ph.D., Faculty of Forestry

This thesis is accepted by the
Dean of Graduate Studies

THE UNIVERSITY OF NEW BRUNSWICK

December, 2021

ABSTRACT

Population expansion and increased activities in the industry have contributed to water contamination. Existing water pollution comes from heavy metals, organic dyes, oils, organic solvents, etc., and raises enormous environmental concerns. Adsorption technology is regarded as an effective method due to its cost-effectiveness, easy operation, and low energy-consuming nature. Considering the removal efficiency, carbon-based material such as graphene oxide is one of the promising candidates. The novel reduced graphene oxide (RGO)-based adsorbents with multiple active sites were prepared by modifying RGO with diethylenetriaminepentaacetic acid (DTPA) in conjunction with polyethyleneimine (PEI). The resultant adsorbents were comprehensively characterized and utilized for removing both positively and negatively charged heavy metal ions at low concentrations including Pb (II), Cu (II), Cr (VI). The removal rate of RGO-(PEI-DTPA) for Pb (II) 2 mg L^{-1}, Cu (II) 3 mg L^{-1} and Cr (VI) 3 mg L^{-1} reached 99 %, 83 % and 99 %, respectively.

DEDICATION

To my mother and father for their endless love, support and understanding during my whole life and especially during difficult times that I suffered emotionally.

To my brother for his eternal love and moral support. He is the one who never left my side.

ACKNOWLEDGEMENTS

Firstly, my utmost gratitude goes to my supervisor Prof Huining Xiao, for his inspiration and encouragement, and his support, guidance. This accomplishment would not be possible without his full support.

I thank the department of Chemical Engineering at the University of New Brunswick for providing financial support for this study.

I would also like to thank all UNB staff that helped me conduct my experiments and perform analyses. I thank Mr. Adon Briggs, Mr. Jason Gorham, and Mr. Carl Murdock Store Manage CHE Department for their continuous technical support.

I cannot find words to express my gratitude to all my dear friends who are always supporting me. Specially, Mr. Linqiang Zheng, Mr. Nur Alam for helping me set my experiments.

I thank Mrs. Sylvia Demerson for their administrative assistance and support during this study.

Table of Contents

List of Tables

List of Figures

List of Symbols, Nomenclature or Abbreviations

GO	Graphene oxide
RGO	Reduced graphene oxide
PEI	Polyethyleneimine
DTPA	Diethylenetriaminepentaacetic acid
SEM	Scanning electron microscope
XPS	X-ray photoelectron spectroscopy
FTIR	Fourier transform infrared spectroscopy
XRD	X-Ray Powder Diffraction
BET	Brunauer-Emmett-Teller
EDS	Energy-dispersive X-ray spectroscopy
ICP-OES	Inductively Coupled Plasma Optical Emission Spectrometer
TGA	Thermo Gravimetric Analyzer
PFO	Pseudo-First-Order
PSO	Pseudo-Second-Order
US EPA	United States Environmental Protection Agency
UV-Visible	Ultraviolet-visible
MB	Methylene blue
MO	Methyl orange

Chapter 1

Introduction

1.1 Background

With increasing industrial or even nonindustrial pollution, water resources contamination has become severe worldwide problem. Natural water is polluted with discharging 2 million tons of wastewater daily, consisting of 70% of domestic sewage, 23% of untreated industrial effluent, and 7% of agricultural waste [1]. There have been a wide range of pollutants in water resources, especially water pollution by heavy metal ions, this has grown concerns because of the toxic nature of these ions on organisms and the possible accumulation in flora and fauna [2]. Several treatment techniques have been utilized for the removal of heavy metal ions, including electrochemical [3], chemical precipitation [4], membrane filtration [5], solvent extraction [6], ion exchange [7], adsorption [8], etc. Each of these methods has its own advantages and disadvantages. For example, membrane filtration, ion exchange, and solvent extraction are expensive methods for treating low concentration of heavy metal ions on a large scale [8]. Electrochemical and chemical precipitation produce large quantities of sludge after treatment which is not cost-effective for disposal.

On the other hand, adsorption can be an ideal substitute due to ease of operation and being a cheap process. In addition, some of the adsorbents in the adsorption can be regenerated in the desorption process and reused for the new adsorption cycle. Numerous materials have been developed to be used as adsorbents for heavy metal removal through the adsorption process. Graphene and its derivatives such as graphene oxide, attracted enormous attention as the next generation materials for the treatment of water dissolved contaminants [9].

1.1.1 Graphene oxide

Graphene oxide is synthesized by chemical oxidation of graphite followed by exfoliation. In this process, several oxygen-containing groups such as carboxylic, hydroxyl, and epoxide functional groups are introduced to the carbon basal plane. The exact chemical structure and composition of GO are still discussed due to different synthesis conditions (time, solvents, exfoliation, etc.)[10]. GO and its composites have attracted tremendous attention for different applications including adsorption of various contaminants such as heavy metals, organic dyes. Pure graphene oxide nanosheets can agglomerate easily which leads to their relatively low adsorption capacity [11]. However, graphene oxide has many oxygen functional groups that could be easily modified to bind to other molecules to enhance its different properties (i.e., adsorption capacity, selectivity, dispersion properties)[12].

1.1.2 Polyethyleneimine (PEI)

Polyethyleneimine is a linear or branched cationic polymer that can be synthesized with different molecular weights. PEI contains a large amount of nitrogen in the form of amino groups on its chains which are effective functional groups for eliminating various pollutants by providing positive charges upon protonation.

PEI finds many applications in functional coatings [13], drug delivery [14], and adsorption [15]. PEI is considered as a metal chelating agent due to the availability of numerous amino groups and has been massively utilized for the retention of heavy metal ions [16, 17]. Two different procedures (crosslinking, modification) are presented to functionalize and produce PEI with different functional groups as well as chelating properties [18]. In this study, crosslinking with

diethylenetriaminepentaacetic acid (DTPA) was used to make it a multifunctional adsorbent for different heavy metal ions.

1.1.3 Diethylenetriaminepentaacetic acid (DTPA)

The synthetic aminopolycarboxylic acids such as ethylenediaminetetraacetic acid (EDTA), nitrilotriacetic acid (NTA), and diethylenetriaminepentaacetic acid (DTPA) are metal chelating agents with a wide range of applications including adsorption, pharmaceuticals, food processing, agrochemicals, etc. The structure contains several carboxylate groups attached to one or more nitrogen atoms which can form stable and soluble complexes with heavy metal ions [19].

It is worth mentioning that global consumption of aminopolycarboxylic acids is approximately 20000 ton yr^{-1}, although some countries like Sweden and Norway banned their consumption because of disruptive effects on aquatic life [20].

1.2 Significance of Study

Very few studies have investigated the preparation and modification of graphene oxide with PEI for wastewater treatment [21-23]. However, none of them explored the effect of binding PEI and DTPA on graphene oxide nanosheets at the same time for removal of both negatively and positively charged heavy metal ions. The as-prepared adsorbents were characterized thoroughly and then used for removal of Pb (II), Cu (II), Cr (VI) heavy metal ions from a synthetic wastewater system at low concentration. Next, adsorption behavior (isotherms, kinetics), pH dependence and recyclability were studied.

The main contributions of this research are as follows:

1. Provide a better alternative to graphene oxide as an adsorbent towards the removal of both negatively and positively charged heavy metal ions.

2. The removal rate of RGO-(PEI-DTPA) nanocomposite for Pb (II) (2 mg L^{-1}) and Cr (VI) (3 mg L^{-1}), Cu (II) (3.1 mg L^{-1}) reached 100 %, 100 %, and 83 %, respectively, and the remaining concentrations after adsorption reached the US EPA standards.

3. Provide a better understanding of different heavy metal ions' adsorption behavior and mechanism in aqueous solutions.

4. The results revealed that RGO-(PEI-DTPA) nanocomposite illustrated the capability of removing anionic and cationic heavy metal ions completely via cooperation mechanism in a low concentration system.

1.3 Objectives

The objective of this work was to modify graphene oxide to synthesize amphoteric adsorbent for removing negatively and positively charged heavy metal ions. This goal was achieved by introducing DTPA with PEI in which both amino and carboxyl groups were introduced simultaneously into graphene oxide nanosheets.

Moreover, the effects of contact time, initial concentration of heavy metal ions and pH on the adsorption behaviour of synthetic materials were discussed thoroughly. Also, the kinetic and isotherm models were fitted to experimental data to understand the adsorption phenomena and mechanism. Finally, the reusability of the adsorbent was examined for evaluating the practicability.

1.4 Thesis Outline

Chapter 2 begins with an explanation about different environmental pollutions and in more specific water pollution and its importance. This section explained about different wastewater technologies and more specifically, wastewater treatment methods for heavy metal removal including adsorption. Furthermore, graphene-based material and its derivative (graphene oxide) as adsorbents were introduced and its modification was discussed.

In chapter 3, the materials and experimental procedure to synthesize GO-based nanocomposites are explained. Also, different characterization techniques that were implemented in this research are introduced including different spectroscopy techniques, adsorption tests, etc.

Chapter 4 evaluates and compares RGO-PEI, RGO-(PEI-DTPA) nanocomposites performance for the removal of different heavy metals Pb (II), Cu (II), Cr (VI) from aqueous solution in a batch adsorption study. The effects of pH, contact time, initial concentration of Pb (II), Cu (II), Cr (VI) solutions on the adsorption performance of RGO-(PEI-DTPA) were discussed. In this chapter, kinetics and isotherms of the adsorption for RGO-(PEI-DTPA) were studied in depth.

Finally, a summary and future work recommendations are presented in chapter 5.

Chapter 2

Literature Review

2.1 Environmental pollution

Environmental pollution happens when contaminants release into the environment excessively and change the global ecosystem, energy pattern, chemical and physical constitution, and abundance of organisms [24, 25]. Three major categories of environmental pollution are air pollution, land pollution, and water pollution. As the name implies, air pollution occurs with the release of toxic chemical into the atmosphere, while in land pollution, toxin goes to the land. Pollutant could be any substance that deteriorate the air, water, or soil quality. Three factors determine the severity of a pollutant: chemical nature, the amount of that chemical, and longevity. This longevity for biodegradable pollutants (i.e., organic wastes, and leftover food) is short and they usually decompose by insects or small birds or convert to nontoxic products through biological activities. On the contrary, non-biodegradable pollutants (i.e., plastics and heavy metals) will remain in the environment and cannot transform into nontoxic materials.

2.2 Water, water pollution and water contaminants

Water is a crucial compound for the life of any kind of creature as well as planet and environment. From all water on the earth, just 3% is fresh water and only 0.01% of this water is available for humans to use [26]. According to World Health Organization (WHO), 700 million people worldwide do not have access to clean water because of unevenly

distributed water resources, worldwide population growth, and bad usage of water management [27]. The deterioration of natural water is among the most significant concerning environmental issues because of its potential effects on human health and ecological and biological systems. For a decade back, the tasteless and odorless water was considered unpolluted and pure but now the whole idea has changed. Water could be clear, although it might contain some impurities like organic pollutants, heavy metal ions, emerging contaminants, etc. [28].

There are two types of water pollutants; point source and non-point source [29]. The United States Environmental Protection Agency (EPA) defines point source pollution as contaminants which directly discharge into water. An example could be operational wastes from industries/factories, treatment facilities. On the other hand, nonpoint-source pollution is when pollutants are released in a wide area mainly occur from run-off from rain or melted snow that could be hard to control [30]. Every day all around the world, over 2 million tons of wastewater are discharged into waterways. For instance, in developing counties, 70% of untreated effluents and 90% of raw sewage are discharged into surface water [31]. The primary source of water pollution are industries including pharmaceuticals, fertilizer factories, petrochemicals, and food industries.

The various types of water pollutants can be classified into several classes, namely; heavy metals, refractory organics, dissolved inorganic, priority pollutants, suspended solids, oxygen- consuming organic matter, etc. [32]. Table 2.1 provides a detailed list of the presented contaminants in wastewater.

Table 2. 1 Summarized the most important pollutants in wastewater [Adopted from Metcalf and Eddy[32]].

Contaminates	Reason for importance
Heavy metal	Heavy metals are usually derived from commercial and industrial activities, even with a low concentration can cause harm to aquatic organisms.
Refractory organics	These materials tend to resist conventional wastewater treatment methods. Examples are surfactants, phenols, and agricultural pesticides.
Dissolved inorganic	Inorganic constituents such as calcium, sodium, and sulfite are usually added to domestic water and can cause a problem if the wastewater is to be reused.
Priority pollutants	They could be organic or inorganic compounds that may be highly toxic, carcinogenic, mutagenic.
Suspended solids	Suspended solids can lead to anaerobic conditions in the aquatic environment. Also, solids interfere with fish spawning, the gravel bed and light penetration cover and consequently making food harder to find.
Oxygen consuming organic matter	If this group is discharged untreated to the aquatic environment, it can lead to depletion of oxygen resources and development of the septic condition.

Generally, heavy metals are defined as metals with a specific gravity of about 5 g cm^{-3} or greater and these could be metals from groups IIA, IIIB, IVB, and VIB of the periodic table. Heavy metal contamination is one of the leading causes of wastewater pollution because of its toxic and carcinogenic nature to aquatic and terrestrial life. A major part of the ground, industrial, agricultural, and even treated wastewater is polluted by different types of metal ions. The presence of heavy metal ions in water or soil causes remarkable damage to aquatic flora and fauna and accumulation at higher levels can even result in death. Approximately twenty different known heavy metal ions were recognized that cause risk for human health. For example, lead ions in water can cause significant risks for nervous systems, brain tissue and in general, human health [33]. The existence of copper ions in water, in a similar way, can lead to liver damage, anemia, etc. [34]. Chromium ions are another group of heavy metal ions present in wastewater that can cause genetic defects

or cancer in living creatures, while Cr (III) is a nontoxic form and can be removed in neutral condition [35]. A mixture of heavy metals is found excessively in air, soil, and more importantly in drinking water [36]. Overall, heavy metal contaminations are becoming one of the most serious problems as result of increasing industrialization and this has made environmental scientists search for effective and economical treatment of heavy metal-bearing wastewaters. National organizations like World Health Organization (WHO), World Bank and National Government Organizations (NGOs) have taken measures to control heavy metal concentration in drinking water and The United States Environmental Protection Agency (US EPA) is regulated heavy metal concentration in drinking water [37].

2.3 Wastewater treatment methods

Given this situation and all the problems that might cause for the environment and human health, measures should be implemented to mitigate the side effects of water pollution. One of the solutions is to reduce and minimize the use of pollutants as pesticides, heavy metals, or other contaminants. Another objective is to design new resources to be able to acquire clean water [38]. For example, reverse osmosis in desalination plant can transform seawater into freshwater, although the process leads to high energy consumption. Finally, it could be a good idea to improve wastewater technologies and equipment to enhance contaminants removal.

Wastewater treatments technologies fall into three basic different groups: physical, chemical, and biological methods (Figure 2.1). Each group of this treatment process has its own advantages and disadvantages.

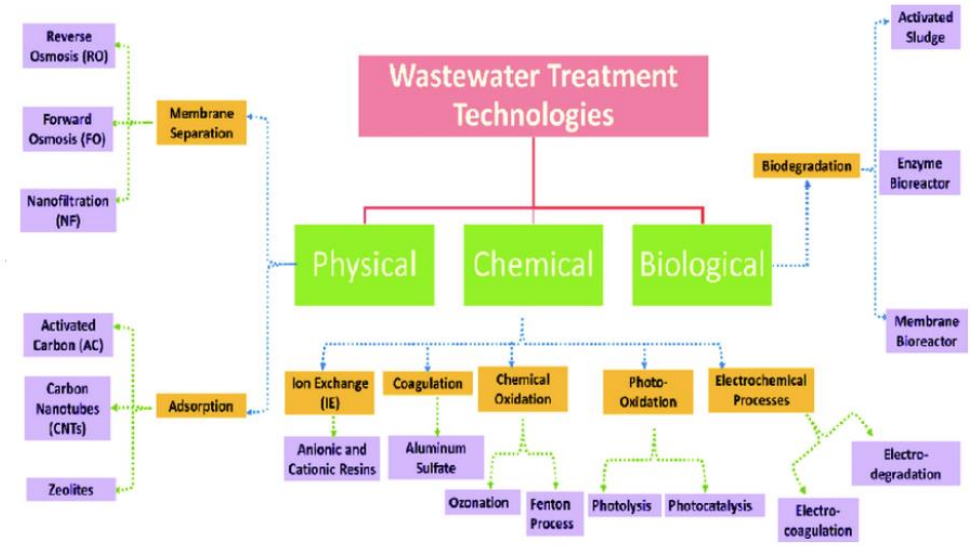

Figure 2. 1 Classification of wastewater treatment technologies [39].

Physical treatment processes consist of various filtration operations including adsorption, membrane separation, flotation, stripping, ion exchange, stripping, distillation in which chemical structures of materials do not change [40]. On the contrary, chemical reactants are utilized in chemical wastewater treatment to separate, destruct, neutralize any kind of contaminants using different techniques such as ion exchange, chemical precipitation, oxidation/reduction [41].

Physicochemical treatment methods are accompanied by low efficiency, high cost, high amount of generated waste material.

Biological wastewater treatment is more economical than physicochemical processes but the removal yield is usually low [42]. In the biological treatment method, water is purified by degrading pollutants into simpler products by microorganisms, fungi, algae, enzymes, etc. [43]. Each of the mentioned technology has its own pros and cons and depending on

the required results; they can be combined in one wastewater treatment unit or used in a selected combination.

2.3.1 Methods for heavy metal removal

To date, many research studies have been done on the development of physical and chemical wastewater treatment technologies and still one economic technology with the capability of reaching desired results is sought. There are various processes to reduce heavy metals concentration in wastewater including: chemical precipitation [44], membrane filtration [45], coagulation-flocculation [46] , ion exchange [47], and adsorption [48]. Chemical precipitation is a promising approach for treating high-concentration heavy metal ions in wastewater to achieve low concentration while complete removal could not be obtained because of precipitated chemicals. Notably, adsorption is used more versatilely owing to low operating cost, high efficiency, ease of operation, large capacity for industrial processing and more importantly, high quality treated water could be obtained [49]. Moreover, adsorbents can be regenerated by the desorption process which is a vital aspect of wastewater treatment.

2.4 Adsorption

Adsorption is defined as a separating process that atoms, biomolecules, molecules from the gas or liquid phase immigrate to the surface of the solid [50]. The adsorbent is a material that is adsorbed, whereas an adsorbate is substance that is being adsorbed. Adsorption usually happens in three consecutive stages as shown in Figure 2.2.

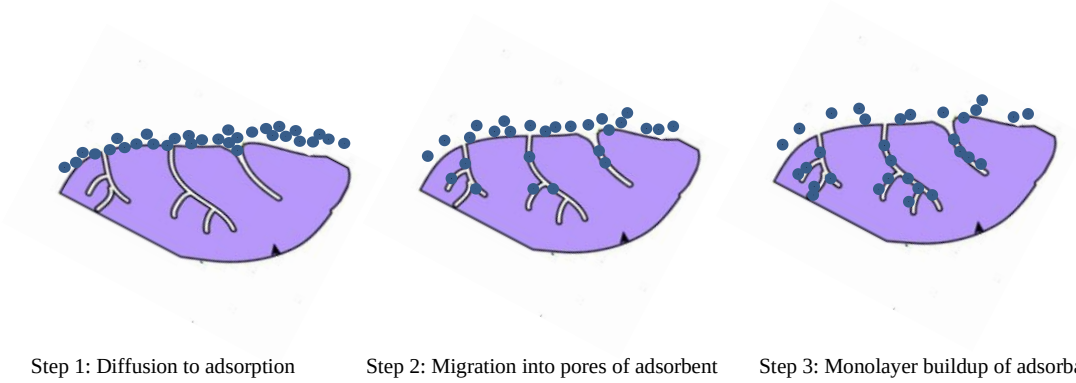

Figure 2. 2 Schematic illustration of proposed adsorption process at the surface of a solid.

1) bulk transfer (film diffusion): in this step, molecules transfer from the liquid or gas phase to external surface of the adsorbent; 2) intraparticle diffusion (solid surface diffusion): substances transfer from the exterior surface into the pores of the adsorbent; 3) surface adsorption: adsorbent materials attach to active sites of interior pores through physical forces or chemical binding [51].

Adsorption based on the interaction type is categorized into two groups: physisorption and chemisorption. Chemisorption has also known as chemical adsorption, is achieved by covalent interactions between the adsorbing material and adsorbate. In contrast, physisorption (physical adsorptions) is caused by the intermolecular force between adsorbates and adsorbents (through van der Waals force attraction) and is a reversible process. Chemisorption adsorption is usually stronger than physisorption adsorption, especially at high temperatures. Figure 2.3 shows a schematic of these interactions.

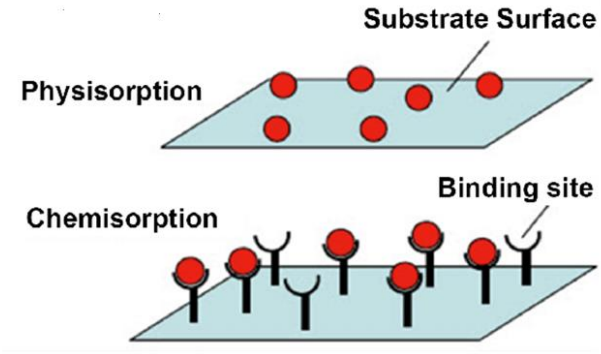

Figure 2. 3 Depiction of physisorption and chemisorption interaction between adsorbent and adsorbate [50].

2.5 Types of adsorbents

Every solid substance can adsorb a sorbate but the adsorption capacity for an adsorbent is determined by many factors such as chemical structure, porosity, specific surface area, and functional groups [52]. Recently, a wide range of adsorbents including carbonaceous materials [53, 54], zeolite [55], clay minerals [56], synthetic polymer materials [57] has been utilized in adsorption technology. Different classifications are presented for adsorbents based on their occurrence, structure, behavior towards the water, etc. Adsorbents are categorized based on their nature in Figure 2.4. Natural adsorbents occur naturally and are considered cheap adsorbents. Examples are zeolites, clay minerals, charcoal, wood, sawdust. Their adsorption capacity can be easily increased by modification [58]. On the other hand, synthetic adsorbents are prepared from raw materials such as household waste, industrial wastes, agricultural waste, sewage sludge and polymeric adsorbents and usually are more expensive than natural types. Among these materials, carbon and its derivatives such as graphene-based material gain enormous interest due to excellent adsorption efficiency.

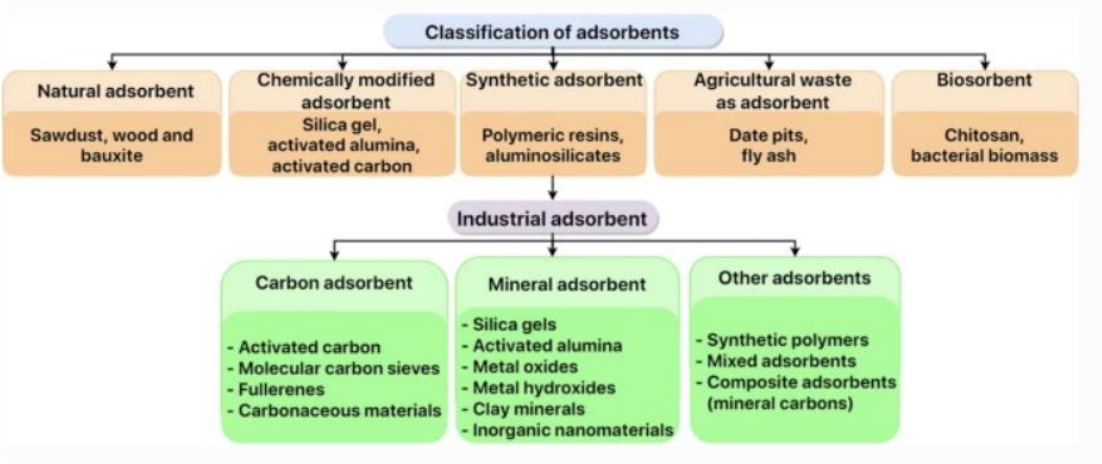

Figure 2. 4 Classification of adsorbents used in the removal of different contaminants [57].

2.5.1 Graphene and graphene-based nanomaterials

Graphene is the simplest form of carbon-based material consisting of sp^2 hybridized carbon atoms arranged in a two-dimensional honeycomb lattice [59]. Graphene was first discovered in 2004 through a process of scotch tape peeling [60], and since then, it has triggered great interest worldwide because of its unique physical-chemical properties such as extraordinary electronic property, perfect mechanical and thermal properties, and high potential adsorption capacity. All these exceptional features make graphene-based material as a promising candidate for different environmental applications in particular water pollution management [61]. Currently, four popular methods (mechanical exfoliation, liquid-phase exfoliation of graphite, epitaxial growth and chemical synthesis) are used to synthesize graphene [62].

However, graphene is not an excellent adsorbent due to several reasons. Firstly, graphene does not have any functional groups on its surface restricting its effectiveness in adsorbing charged pollutants such as heavy metals and dyes in the water. Also, graphene has poor

dispersion in water related to π-π stacking of aromatic rings which restrict its specific surface area that can interact with aromatic pollutants. Meanwhile, the mentioned properties can be further enhanced by the oxidation reaction of graphene to synthesize GO. Until recently, GO is mainly synthesized by well-known methods, typically including chemical oxidation and exfoliation of graphite (i.e., Brodie method, Staudenmaier method, Hofmann method, Hummers method or some variation of these methods). The reaction consisting of oxidation graphite to graphite oxide and subsequently an exfoliation to GO is shown in Figure 2.5. The potassium chlorite and nitric acid were the first reported oxidizing agents for preparing GO in 1859. After that, Staudenmaier, in 1898 mixed graphite with a mixture of nitric acid, concentrated sulfuric acid and potassium perchlorate to increase the acidity. This method was more practical than previous ones but was found to be a hazardous and time-consuming approach. Hummers and Offeman in 1958 introduced a commonly used method for GO synthesis by mixing graphite with concentrated sulfuric acid, sodium nitrate, and potassium permanganate [63]. The key reactant in a synthetic method is dimanganese heptoxide (Mn_2O_7) formed from potassium permanganate and sulfuric acid reaction. The properties and structure of a synthetic GO are highly dependent on the synthesis method, degree of oxidation, purification method, type and grade of graphite [64].

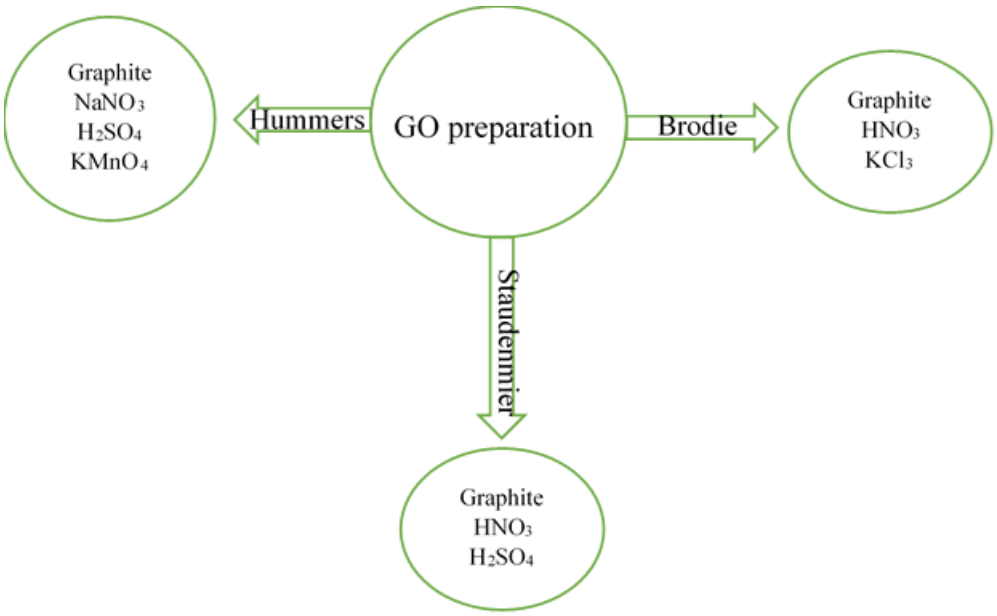

Figure2. 5 Different synthesis methods for preparation of GO using graphite.

GO has a graphitic-layered structure that a monolayer of carbon atoms arranged in a honeycomb crystal plane; and the intercalation of oxygenous functional groups causes the increase of interlayer distance (d-spacing obtained from XRD characterization) from 0.4 nm to 0.87-1.1 nm [63]. This increase can weaken the van der Waals forces between the graphitic layers, thus facilitating the exfoliation of GO layers. The incorporation of epoxy, carboxyl and hydroxyl groups on both sides of the sheets increases the typical thickness of monolayer GO sheet compared to graphene sheet.

The oxygenous functional groups render GO sheets hydrophilic and highly negative charged, which could be exploited in adsorption applications. The anionic carboxyl and hydroxyl groups that existed on the GO plane can act as anchoring sites for metal ion complexation, thereby improving the adsorption of multivalent metal ions. These functional groups are also reactive and can be used as grafting sites to have ionic, hydrogen

bonding, and covalent interactions with other molecules to facilitate adsorption. Furthermore, the large delocalized π-electron system of GO nanosheets allows the π - π interactions with organic dyes with aromatic structures. Thus, Graphene oxide as a group of carbonaceous material set a good example of promising adsorbent that has been extensively used to remove different pollutants with different charges such as heavy metals and organic dyes.

In addition to the aforementioned characteristics enabling GO to be an effective material to improve the performance of nanocomposites, GO itself has superior properties such as high mechanical properties, good biocompatibility, which make GO more suitable as a super adsorbent compared to graphene [65]. In recent years, GO has become increasingly important for environmental application on account of mentioned features that render GO superior advantageous over other nanomaterials.

Meanwhile, oxygen-containing groups on GO plane and its π-π stacking structure cause self-stacking and agglomeration that reduce the surface area of the GO substantially and consequently lead to low adsorption capacity and limit its practical usage of GO in pollution management. To overcome mentioned shortcomings, various polymers have been grafted onto the GO surface to improve the dispersion and adsorption performance of GO.

2.6 Modification of GO

Graphene oxide nanosheets (with chemically reactive functional groups) as a substrate are easily modified with other reagents (with carboxyl, amino, sulfhydryl groups) to produce

advanced adsorbent with enhanced adsorption rate, adsorption capacity, and dispersion properties.

Modification on GO nanosheets could be non-covalent (van der Waals interaction and hydrogen bonding) or covalent interactions or a combination of both [66]. In non-covalent interaction, surface charge and electrical properties of graphene oxide are usually enhanced, while in covalent interaction methods mechanical properties and stability are enhanced.

In a covalent bonding reaction, carboxyl or hydroxyl groups of GO nanosheets bind with molecular or polymeric species [67]. Furthermore, epoxy groups on GO basal plane can have ring-opening reactions with organic molecules [68]. In this approach, the physiochemical, mechanical properties, adsorption performance, and other properties are improved [69].

Amino groups are considered as useful functional groups for the elimination of heavy metals particularly Cr (VI) from wastewater. In recent years, many attempts have been made to functionalize GO with an organic compound with amino groups. However, the content of N in some of these organic molecules such as (3-Aminopropyl)triethoxysilane is relatively low and does not show ideal adsorption capacity [70].

Polyethyleneimine (PEI) is a hydrophilic polymer that contains a large quantity of primary, secondary, tertiary amine groups on its linear structure and could interact strongly with anionic metal ions including Cr (VI). Also, it has high selectivity and strong metal chelating ability which can improve graphene oxide adsorption capacity. If PEI is attached to the GO, this attachment can effectively reduce or prevent agglomeration of the GO nanosheets.

Also, the residual amine groups of the PEI can exhibit good adsorption capacity for negatively charged organic or inorganic ions.

Recently, PEI has been adopted to graphene oxide to synthesize different forms of nanostructures (hydrogel, aerogel, membrane, etc.) for water remediation [16, 21, 22, 71]. The next section summarized publications on preparing different forms of GO-PEI for the adsorption application. Geng et al. developed a facile and cost-effective route to prepare GO-PEI hydrogel with significantly enhanced adsorption capacity 436.2 (mg g^{-1}) towards Cr(VI) in comparison with untreated GO and RGO [71]. In another study, self-assembly method was used to produce GO-PEI hydrogel in an aqueous acidic medium for Hg remediation and the observed excellent adsorption performance was attributed to the synergistic effect resultant from the interactions between GO and PEI, giving a high content of N-rich groups and negative zeta potential over a wide pH range [21]. Moreover, self-assembly method was utilized for preparing GO-PEI hydrogel with high adsorption capacity (898 mg g^{-1}), high removal rate (>90% at ppm level) and high selectivity of uranium [71].

In a different study, three-dimensional GO-PEI was synthesized by a self-assembly method and used for the simultaneous elimination of cationic U (VI) and anionic Re (VII). The maximum adsorption capacity of GO–PEI composites at pH 5.0 for U (VI) and at pH 3.5 for R (VII) was determined to be 629.5 mg g^{-1} and 262.6 mg g^{-1}, respectively [72].

GO-PEI nanocomposite was also used for removing anionic and cationic dyes, the constructed aerogels were fabricated via an optimized sol-gel method and showed high adsorption capacity for anionic MO (331.0 mg/g) at pH 2.0 while for cationic MB (249.6 mg/g) at pH 10.5 [73].

Xi et al. synthesized adsorbent by anchoring DTPA grafted PEI onto carboxylated GO, which exhibiting good adsorption capacities against both heavy metal ions (Pb (II), Cu (II)) and organic dye (MB) in an aqueous solution [74].

GO with oxygen-containing functional groups is a promising adsorbent to remove cationic pollutants from water. A literature analysis demonstrated that adsorbents with a high density of amino and carboxyl groups can have a high removal rate for anionic and cationic heavy metal ions respectively. This removal rate and adsorption capacity are enhanced with increasing functional groups density [71]. To achieve high removal efficiency of both anionic and cationic pollutants, PEI-DTPA was associated with GO to fabricate amphoteric adsorbent.

In this work, we synthesized two different adsorbents namely RGO-PEI, RGO-(PEI-DTPA).

The adsorption behavior of RGO-PEI nanocomposite was evaluated in different publications for different heavy metal ions as well as organic dye removal so far [17, 71, 75]. The novelty in this work is to attach DTPA into GO and PEI that could contain both high amino and carboxyl functional groups for efficient and fast removal of low-level concentrations of Cr (VI), Pb (II), Cu (II) in synthetic wastewater. The presence of DTPA and PEI on the GO nanosheets render plentiful active sites for the adsorption of both anionic and cationic metal ions.

Chapter 3

Methodology

3.1 Materials

Graphite powder (flake) was obtained from Aladdin. Polyethyleneimine (PEI, MW~800, 99%), potassium dichromate, sodium nitrite, potassium permanganate, hydrogen peroxide, sulfuric acid, diethylenetriaminepentaacetic acid (DTPA), zinc sulfate, lead nitrate, sodium hypophosphite (SHP), sodium hydroxide, and hydrochloric acid were all purchased from Sigma Aldrich. All of them were analytical grade reagents and were directly used without any purification.

3.2 Methods

3.2.1 Preparation of GO

GO nanosheets was prepared according to a modified Hummers' method [76, 77]. Briefly, 1 g of graphite powder was mixed with 120 mL of concentrated sulfuric acid for 2 h. After that, 1 g of sodium nitrate was added and constantly mixed the fine dispersion. 6 g of potassium permanganate were slowly added to the solution with a temperature below 20°C (pink color). This mixture was stirred for about 72 h at ambient temperature (brown color). In the next step, hydrogen peroxide was gradually added to the mixture in 600 mL of distilled water until reaching bright golden yellow color. The solid product was centrifuged with a mixture of distilled water and hydrochloric acid repeatedly to remove any impurities. Finally, probe ultra-sonication was utilized to exfoliate graphene oxide nanosheets in water

[78]. Figure 3.1 shows the graphical representation and chemical structure of synthesizing graphene oxide.

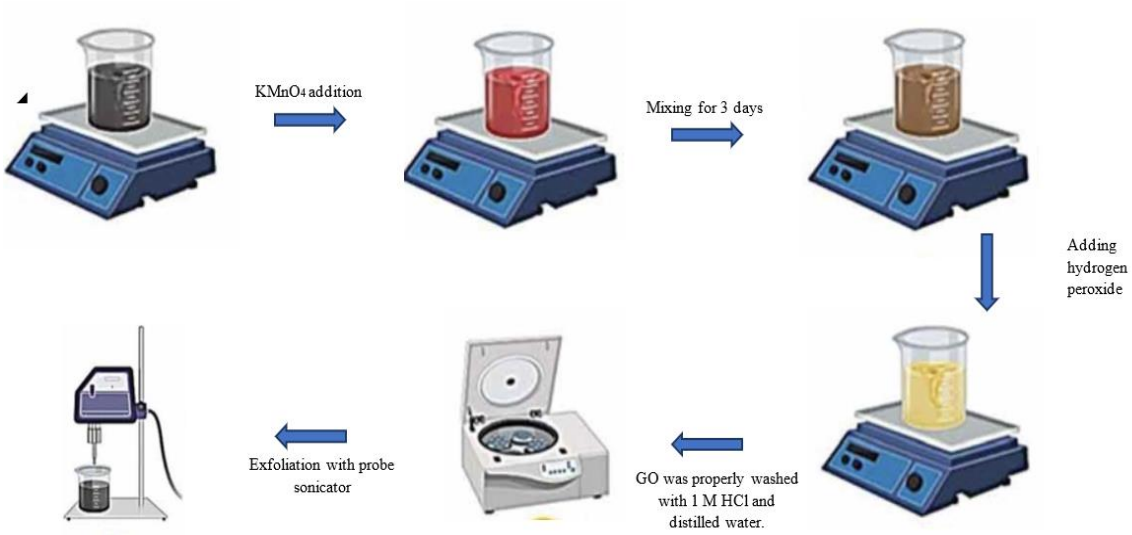

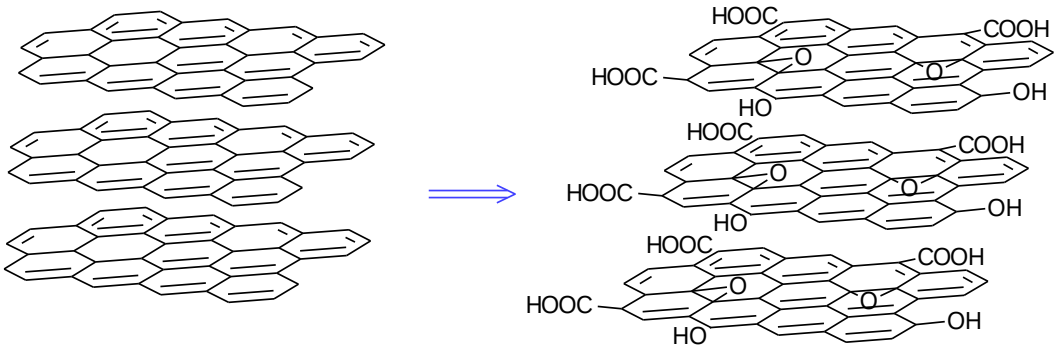

Graphite

Graphite oxide

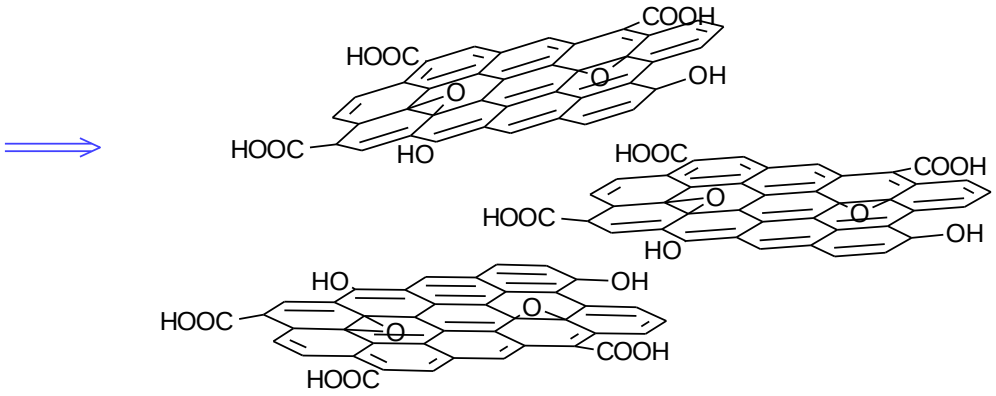

Graphene oxide

Figure3. 1 Graphical representation and chemical structures of synthesis of graphene oxide from graphite [79].

3.2.2 Preparation of RGO-PEI

The pH value of exfoliated GO in distilled water was adjusted to 9.0 with sodium hydroxide solution and then GO dispersion (0.78g of GO in 10 mL of water) mixed with PEI (2.34 g) and heated in the water bath at 60°C for 8 h. The as-prepared product was washed in distilled water repeatedly to remove impurities like non-reacted PEI and sodium hydroxide. RGO-PEI nanocomposite was obtained after lyophilization without pre-freezing. The reaction is shown in Figure 3.2.

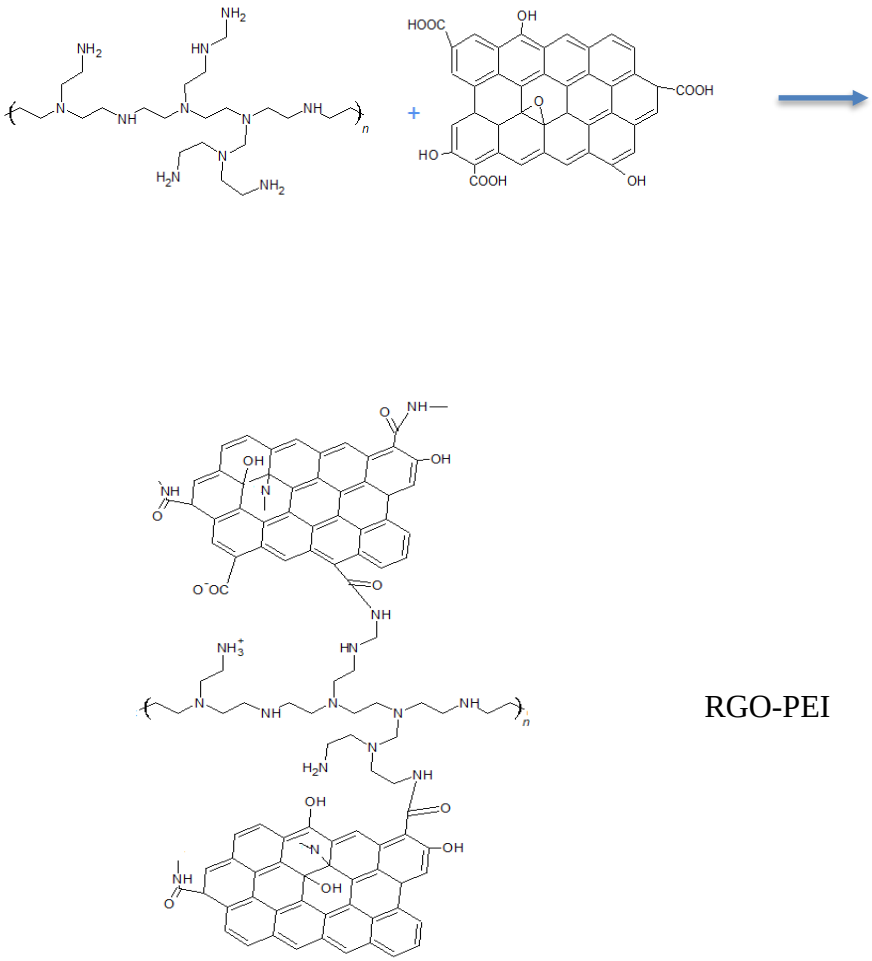

Figure3. 2 Schematic demonstration for RGO-PEI synthesis.

3.2.3 Preparation of RGO-(PEI-DTPA)

Firstly, PEI-DTPA was synthesized by mixing and dissolving 1 g of the DTPA with 0.76 g of PEI in 2 mL of alkali solution. In the next step, sodium hypophosphite was added to the prepared solution and was heated at 105°C for 4 h. The obtained yellow liquid was named PEI-DTPA.

Secondly, 2.1 g of PEI-DTPA solution was added to 0.7 g of GO nanosheets in 10 mL water (with an adjusted pH value of 9) and intensely stirred at 60°C for 8 h. After 8 h, GO nanosheets and PEI-DTPA were crosslinked, and then washed with distilled water several times to remove all unreacted molecules. Finally, synthetic nanocomposite was obtained after lyophilization without pre-freezing. Graphene oxide-based amphoteric adsorbent was formed and the structure is illustrated in Figure 3.3.

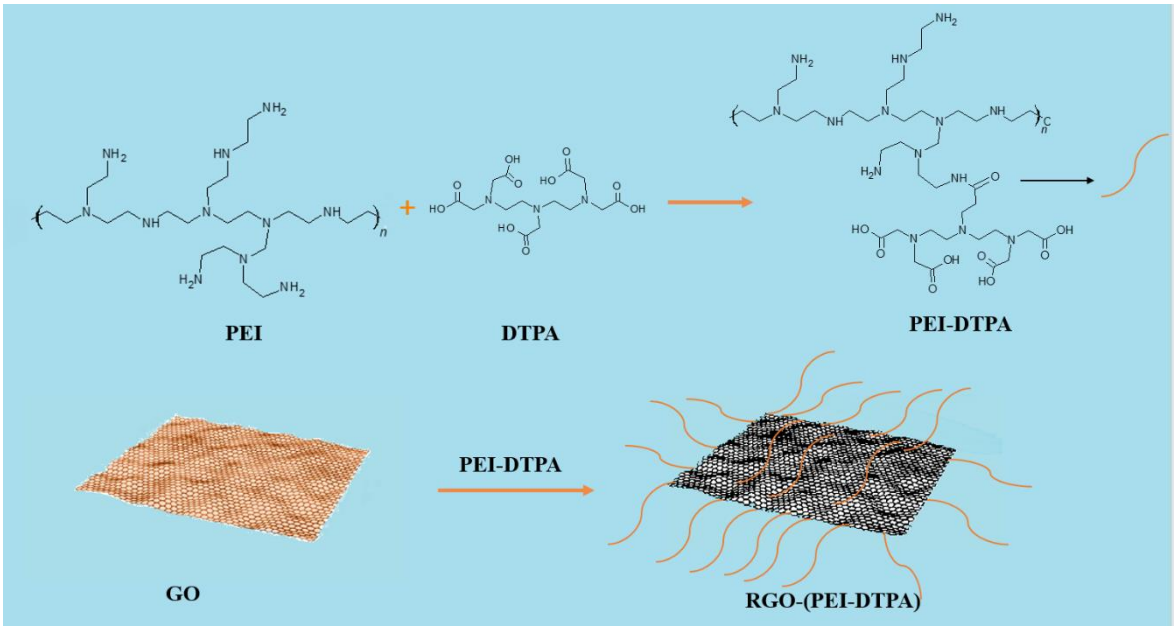

Figure3. 3 Illustration of the synthesis process of RGO-(PEI-DTPA).

3.3 Characterization and analysis

A variety of analytical techniques such as Fourier transform infrared spectroscopy (FT-IR), UV-Visible Spectroscopy, Scanning electron microscopy (SEM), X-ray diffraction (XRD), Thermogravimetric (TG), X-ray photoelectron spectroscopy (XPS), Brunauer-Emmett-Teller (BET), and Zeta potential have been used to reveal structural, elemental or morphological properties of synthetic materials.

The surface functional groups of synthetic nanocomposites were observed by FTIR. FTIR spectra were recorded on Nicolet 6700 FTIR spectrometer (Thermo Scientific, USA) using KBr powder to determine the formation of new chemical bonds between GO and PEI and DTPA structures. UV–vis measurements were taken with Evolution 201 (Thermo Scientific, USA) spectrophotometer in wavelength rang of 200–800 nm in distilled water.

The surface energy and surface chemical composition of the synthetic nanocomposites can be further investigated by K-Alpha XPS (Thermo Scientific, USA), confirming the strong interaction between GO and PEI/DTPA materials in terms of the variation of the binding energies.

The specific surface area (BET) was measured with a (Belsorp-Max BEL Inc, Osaka, Japan) instrument.

The powder diffraction patterns of samples (GO film or fine particle of synthetic materials) were collected on a Bruker AXS D8 Advance solid-state powder diffraction XRD system with Cu Kα radiation (λ= 0.1542 nm) at 45 kV and 100 mA. Thermogravimetric analysis (TGA) of the magnetic adsorbents were performed using SDT Q600 by TA Instruments, (USA) fitted with nitrogen gas supply. The equipment was operated between 10 °C to 600 °C at a 5 °C min^{-1} heating rate. A JEOL JSM6400 Scanning Electron Microscope (SEM)

equipped with an EDAX Genesis 4000 Energy Dispersive X-ray (EDS) analyzer was used to observe surface and cross-sectional morphologies and chemical compositions of before and after adsorption samples. Zeta potential represents the surface charge characteristics of a nanocomposite in aqueous solution, which can determine whether nanocomposite is conducive to positively charged pollutants or negatively ones and was done by Zeta potential analyzer (ZetaPlus, Brookhaven Instruments Corporation, USA).

3.4 Adsorption and desorption experiments

The batch adsorptions of Cr (VI) and Cu (II), and Pb (II) on RGO-PEI, RGO-(PEI-DTPA) nanocomposites were carried out to study the effect of initial concentration, initial pH solution, and contact time. A stock solution of each metal ion was diluted to prepare the different adsorbate solutions at varying concentrations. The adsorbent (0.05 g) was dispersed into 50 mL of each heavy metal aqueous solution and was shaken in a temperature-regulated shaker (SWB25) (German Thermo Electron Corp) and agitated at 150 rpm for 5 h unless special condition explains and the results were averaged. To study the time effect on the adsorption, a certain amount of solid/liquid mixture was taken out at different time intervals and separated quickly through 0.45 μm filter at a predetermined time interval.

The pH values of Cr (VI), Cu (II), and Pb (II) solutions were regulated using HCl solution (1.0 mol L^{-1}) or NaOH solution (1.0 mol L^{-1}). The samples after adsorption experiments were filtered through 0.45 μm filter and Cu (II) and Pb (II) concentration was determined by inductively coupled plasma optical emission spectrometry (Varian Vista MPX Axial). Cr (VI) concentration was measured by a diphenylcarbazide method (DPC) on UV–vis spectrophotometer (Evolution 201, Thermo Scientific, USA) at 540 nm.

The removal efficiency (R%) can be calculated according to equation (3.1):

$$\text{Removal (\%)} = \frac{(\text{Co} - \text{Ce})}{\text{Co}} \times 100 \qquad \text{Equation 3.1}$$

where C_o (mg L^{-1}) is the initial heavy metal ion concentration in the solution, C_e (mg L^{-1}) is the heavy metal ion concentration at the equilibrium.

Competitive adsorption experiment was conducted in binary mixtures with each concentration of all the metal ions at 5 mg L^{-1} (pH 7, contact time 5 h).

The metal ion loading capacity (q) was determined using equation (3.2):

$$q = \frac{(Co - Ce) \times V}{m} \qquad \text{Equation 3. 1}$$

where q (mg g^{-1}) is the quantity of metal ions removed from solution per gram of each absorbent, m (g) is the absorbent mass, V (*L*) is the metal ion solution volume, C_o (mg L^{-1}) is the initial heavy metal ion concentration in the solution, C_e (mg L^{-1}) is the heavy metal ion concentration at the equilibrium.

3.4.1 Adsorption Kinetic Models

Adsorption kinetics is one of the most valuable tools to explore the adsorption mechanism, rate-controlling steps in adsorption, and adsorption equilibrium. The information obtained from kinetics provides the feasibility of practical applications of GO-based nanocomposite in wastewater treatment. Two popular models were adopted in describing the adsorption processes of pollutants by graphene oxide based adsorbents, i.e., pseudo-first-order (PFO)

kinetic model, pseudo-second-order (PSO) kinetic model. The results were obtained by mixing 0.05 g of RGO-(PEI-DTPA) nanocomposite with 50 ml of heavy metal ion solution at room temperature and pH 7.

The non-linear forms of the PFO and PSO kinetics are presented in equations 3.3 and 3.4 respectively.

$$q_t = q_e(1 - e^{-k_1 t}) \qquad \text{Equation 3. 2}$$

$$q_t = \frac{k_2 q_e^2 \, t}{1 + k_2 q_e t} \qquad \text{Equation 3. 3}$$

In these equations, q_t and q_e are the sorption capacities (mg g^{-1}) at time t and equilibrium respectively; K_1 (min^{-1}) and K_2 (g mg^{-1} min^{-1}) are the pseudo-first-order rate constant and pseudo-second-order rate constant, respectively.

3.4.2 Adsorption Isotherm Models

Two isotherm models (Langmuir, Freundlich) were used to describe the adsorption phenomena of contaminants on GO based nanocomposites. The isotherms were obtained by mixing RGO-(PEI-DTPA) nanocomposite (0.05 g) with each metal solution (50 mL) at varying initial concentrations (2-10 mg L^{-1}) at room temperature and pH 7.

The Langmuir isotherm was proposed for the first time to explain the adsorption of hydrogen on a solid surface [80]. This model was established based on three assumptions. Firstly, the adsorbent consists of a homogeneous surface. Secondly, the molecules are adsorbed in a monolayer coverage on the surface and lastly, the adsorbate in the form of

gas does not have any lateral interactions within the monolayer [80]. Based on mentioned assumptions, the model is given by equation 3.5.

$$\frac{1}{q_e} = \frac{1}{q_m} + \frac{1}{C_e\, q_m K_L} \qquad \text{Equation 3. 4}$$

In this equation, q_e (mg g^{-1}) is the equilibrium amount of adsorbed metal ion on the adsorbent, q_m (mg g^{-1}) is the maximum adsorption capacity, C_e (mg L^{-1}) represent the concentration of metal ion at equilibrium and K_L (L mg^{-1}) is defined as Langmuir adsorption constant. K_L values are related to the adsorption affinity of a particular adsorbate; and a higher number of K_L represents the greater affinity of the adsorbate species to the adsorbent. R_L is a dimensionless separation that is defined for Langmuir equation and is given by the following equation.

$$R_L = \frac{1}{(1+C_0\, K_L)} \qquad \text{Equation 3. 5}$$

Where C_0 (mg L^{-1}) is the highest initial metal ion concentration. R_L determines whether adsorption is favorable ($0 < R_L < 1$), unfavorable ($R_L > 1$), irreversible ($R_L=0$) or linear ($R_L= 1$).

The Freundlich isotherm model is another isotherm model to describe the experimental adsorption data. The linear form of the equation is presented in equation 3.7.

$$LOGq_e = LOG_{K_F} + \frac{1}{n} LOGC_e \qquad \text{Equation 3. 6}$$

Where K_F (mg g^{-1}) represents the Freundlich constant related to adsorption affinity, C_e (mg L^{-1}) is the equilibrium concentration of adsorbate, q_e (mg g^{-1}) is equilibrium amount of adsorbed metal ion on the adsorbent and 1/n is isotherm constant which can represent adsorption intensity.

The Langmuir isotherm model assumes that sorption occurs at specific sites, which are distributed uniformly across the surface of adsorbent, while the Freundlich model assumes a heterogeneous sorption surface area and active sites with varying energy based on a multi-layer sorption process.

3.4.3 Adsorbent regeneration

The desorption experiment was carried out with HCl (0.1 mol L^{-1}) or NaOH (0.1 mol L^{-1}) solutions. After reaching equilibrium adsorption, the adsorbent was filtered through 0.45 μm membrane filter. 0.05 g of the adsorbent was mixed with 50.0 mL of HCl solution (0.1 mol·L^{-1}) to desorb heavy metal ions for 1 h and then using NaOH solution (0.1 mol·L^{-1}) at 150 rpm at room temperature for 1 h. Finally, the solid material was washed with distilled water to reach neutral pH and dried overnight at 60 ˚C in a temperature-controlled oven.

Chapter 4

Results and discussion

4.1 Optimization of PEI-DTPA loading on the GO nanosheets

The amount of PEI-DTPA anchored on GO nanosheets is an important factor in regulating adsorption capacity. It is well known, higher loading of PEI-DTPA can enhance the adsorption capacity for heavy metal uptake. However, a large amount of grafting could lead to a decrease of adsorptive sites and consequently lower adsorption capacity. Thus, it is crucial to optimize the PEI-DTPA ratio. Different amounts of PEI-DTPA (0.3 g, 0.6 g, 0.9 g, 1.2 g, 1.5 g) were introduced on GO nanosheets (0.3 g) and the resultant composites were termed as RGO-(PEI-DTPA), RGO-2(PEI-DTPA), RGO-3(PEI-DTPA), RGO-4(PEI-DTPA), RGO-5(PEI-DTPA), respectively. The results in Figure 4.1 demonstrated that adsorption capacity for Cr (VI) increased from RGO-(PEI-DTPA) to RGO-3(PEI-DTPA), relating to the increasing of chelation sites. There was a decrease in adsorption capacity for RGO-4(PEI-DTPA), RGO-5(PEI-DTPA) nanocomposites, which might be attributed to declining of the exposed adsorptive site on the surface of the adsorbent or the over-stacking of GO nanosheets and self-aggregation of PEI-DTPA induced by the excessive PEI-DTPA. Therefore, RGO-3(PEI-DTPA) was chosen as an optimized adsorbent and in this study, nanocomposites were synthesized based on 1:3 (RGO: PEI/PEI-DTAP) ratio and abbreviated as RGO-(PEI-DTPA) and RGO-PEI. It is worth mentioning that the optimization experiment was not performed for cationic heavy metal removal. This is because the amount of amino and carboxyl groups from acid-base titration

on PEI-DTPA were 4.75 mmol g^{-1}, 6.38 mmol g^{-1} respectively; and a lower number of amino groups could be a limiting factor for anionic heavy metal removal. Therefore, the optimization experiment was only done for anionic heavy metal removal.

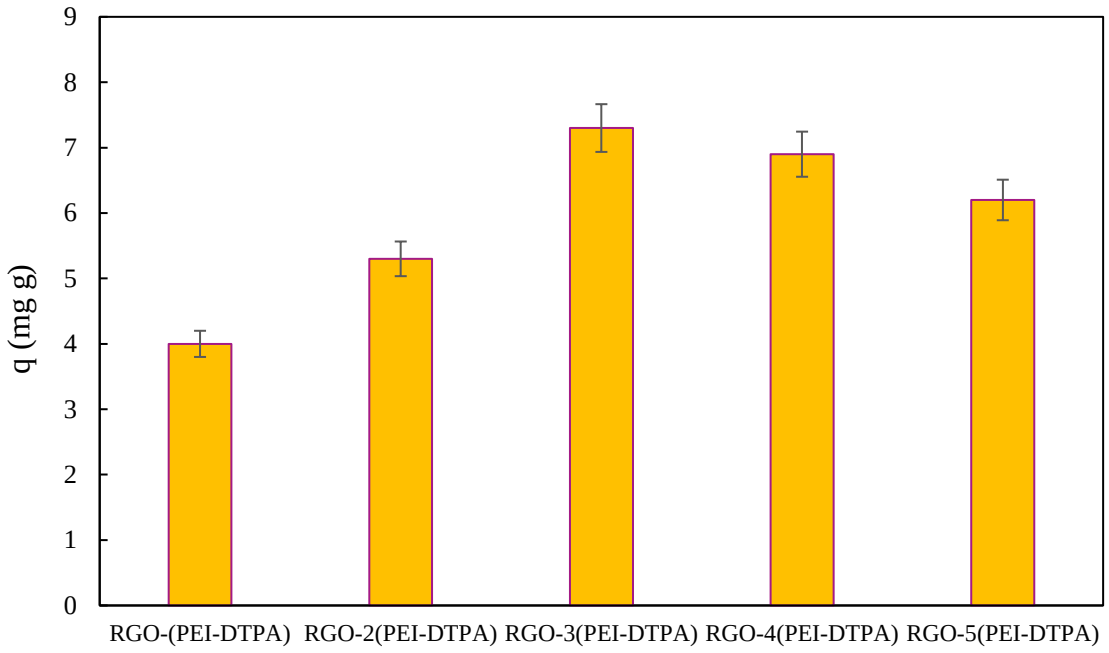

Figure 4. 1 Effect of the content of PEI-DTPA on adsorption capacity: Cr(VI) ion concentration 10 mg L^{-1} , adsorbent dosage 1 g L^{-1}, room temperature, stirring speed 150 rpm, contact time 5 h.

4.2 Chemical characterization and morphological analysis of synthetic materials

The chemical structures of GO, RGO-PEI, and RGO-(PEI-DTPA) nanostructures were investigated by XRD, FT-IR, UV–vis spectroscopy, and XPS. The XRD pattern of GO, RGO-PEI, RGO-(PEI-DTPA) are shown in Figure 4.2.

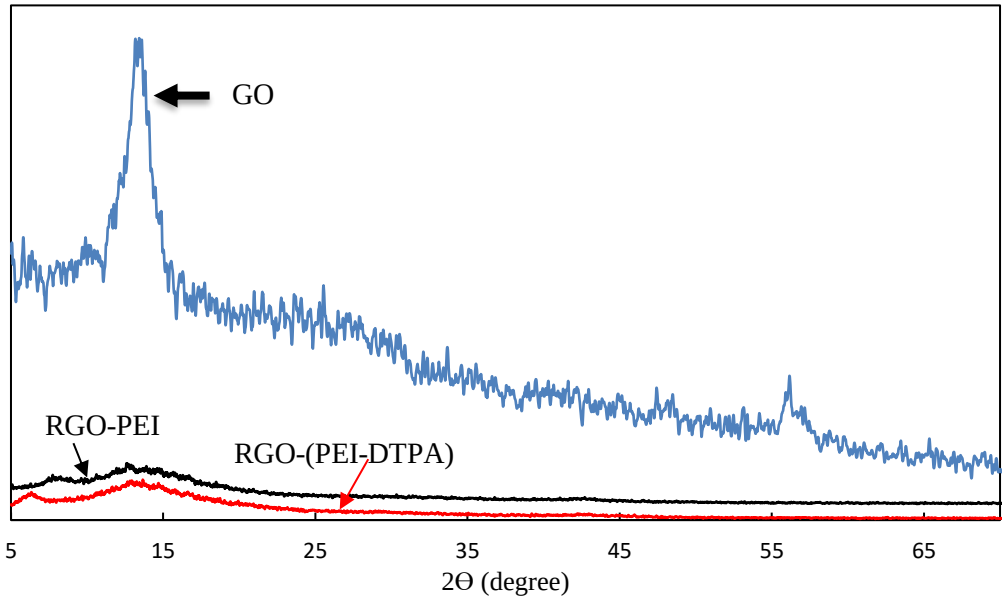

Figure 4. 2 XRD patterns of GO, RGO-PEI, RGO-(PEI-DTPA).

The XRD pattern of GO exhibits a sharp peak (001) at $2\theta = 13.4°$, corresponding to the interlayer d-spacing of 0.84 nm of GO sheets. This interlayer spacing is strongly determined by two factors: the amount of adsorbed water molecules on adjacent GO nanosheets and the number of oxygen-containing groups. From the comparison of XRD patterns, it can be observed that the strong diffraction peak at $2\theta = 13.4°$ in GO pattern disappeared in RGO-PEI, RGO-(PEI-DTPA) nanocomposites, and broad and weak peaks appeared around 13°. These changes might be related to the successful grafting of PEI and PEI-DTPA onto GO nanosheets, which broadens the interlayer distance of GO and weakens the crystal structure of GO (because of the amorphous state of crosslinked PEI/PEI-DTPA). Also, the amidation reaction between the carboxyl group in GO nanosheets and the amino group in PEI chains creates defects on the GO nanosheets surface

[81]. The XRD results strongly confirmed that PEI and PEI-DTPA molecules successfully modified GO nanosheets.

To further investigate the possible interactions between GO and PEI/DTPA, FT-IR spectra were recorded for GO, RGO-PEI, RGO-(PEI-DTPA) nanocomposites; and are shown in Figure 4.3. For GO, a broad and wide characteristic peak around 3407 cm^{-1} belongs to O-H stretching vibration of hydroxyl groups. The bands at 1716 cm^{-1}, 1623 cm^{-1}, 1253 cm^{-1} are assigned to stretching vibration in carboxyl group, skeletal vibrations from unoxidized graphitic domains, C-O-C of epoxide group [82, 83]. These characteristics bands of oxygen-containing groups confirm that GO was successfully synthesized. Compared to pure GO, in RGO-PEI nanocomposite, -CONH- and -NH as amide bands appeared at 1635 cm^{-1}, 1558 cm^{-1}, whereas C=O of carboxylic acid groups disappeared. The results suggest that amine groups of PEI were successfully reacted with carboxyl groups and formed amide groups. Moreover, C-O-C of epoxide groups (at 1253 cm^{-1}) were weakened in RGO-PEI and RGO-(PEI-DTPA), implying there was a ring-opening reaction between amine groups of PEI or PEI/DTPA and epoxy groups of GO. Another observed peak at around 1085 cm^{-1} is assigned to C–N bond stretching vibrations. Also, a new characteristic peak appears at 1456 cm^{-1}, which was related to secondary amino from the PEI that can be seen in both RGO-PEI and RGO-(PEI-DTPA) nanocomposites. These results confirm that GO reduced during the reaction and PEI molecules were effectively attached to reduced graphene oxide. In the FTIR of RGO-(PEI-DTPA) a shoulder at 1733 cm^{-1} was appeared again due to the existence of carboxyl groups from DTPA. It is also concluded that, incorporating PEI or PEI/DTPA molecules into GO nanosheets facilitates the transformation of hydrophobic reduced graphene oxide to hydrophilic reduced RGO-PEI or RGO-(PEI-DTPA)

nanocomposites. Based on the FTIR spectra, these results confirm that the PEI and PEI-DTPA molecules are attached successfully onto graphene oxide nanosheets.

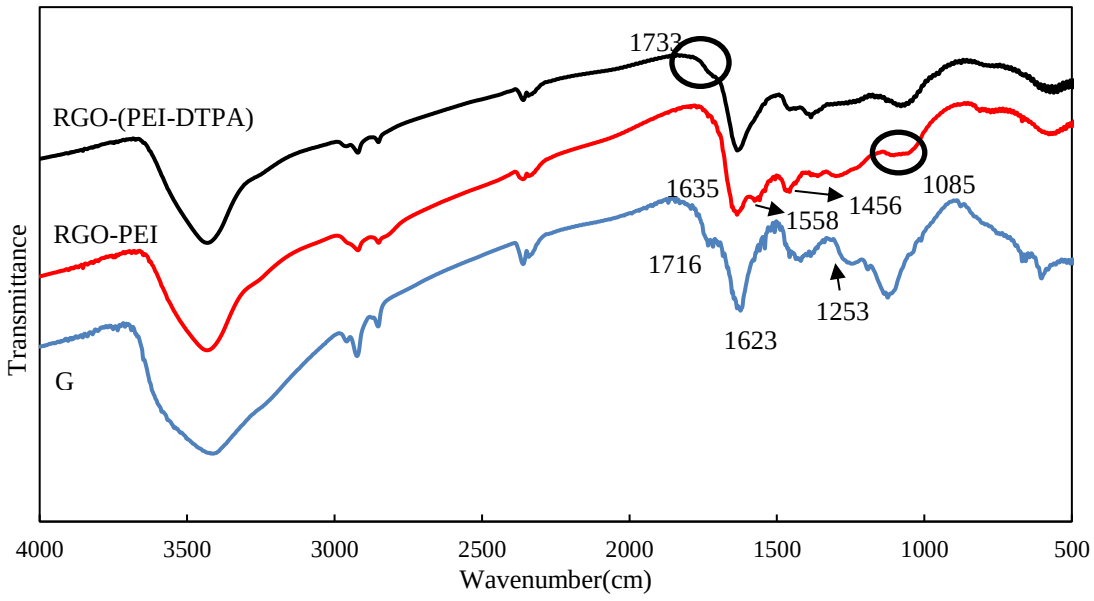

Figure 4. 3 FTIR spectra of GO, RGO-PEI, RGO-(PEI-DTPA).

As the reaction proceeded, the color of the mixture of GO and (PEI or PEI-DTPA) solutions was gradually changed from brownish yellow to black. This color-changing is the sign demonstrates the GO simultaneously functionalized and partially reduced by amine groups of PEI or PEI-DTPA. This also can be seen in UV-visible spectra where GO nanosheets exhibits two characteristic peaks, a strong peak around 237 nm corresponding to π-Plasmon transition of aromatic rings and a shoulder around 300 nm that is attributed to $n \rightarrow \pi^*$ transition of the carbonyl groups. All the data are in good agreement with previous publication and are shown in Figure 4.4 [84]. The shift in absorption peak of RGO-PEI is due to the restoration of π electron conjugation within the graphene sheets [85].

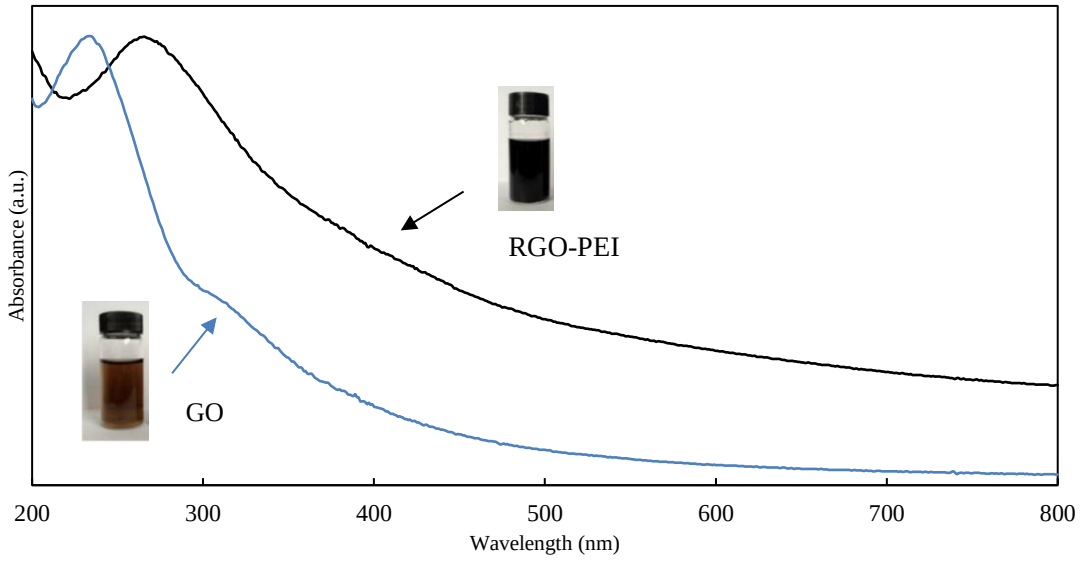

Figure 4. 4 UV-vis spectra of pure GO and RGO-PEI in distilled water.

The surface chemical structure of RGO-(PEI-DTPA) was also analyzed based on the XPS data, as shown in Figure 4.5. Wide scan spectra of RGO-(PEI-DTPA) show O1s, N1s, C1s signals which confirm that nitrogen molecules from PEI-DTPA are attached to graphene oxide structure (Figure 4.5 a). The O 1s XPS spectra of RGO-(PEI-DTPA) is illustrated in Figure 4.5 b and the peaks at 532.33 eV and 531.08 eV were attributed C-O-H and C=O. The characteristic peaks of N species in RGO-(PEI-DTPA) at ~400 eV can be curve-fitted into various N groups including primary, secondary, and tertiary amino groups and amides which are shown in Figure 4.5 c. The above results are consistent with the characterization results of FTIR.

All these results demonstrate the successful preparation of RGO-(PEI-DTPA) and they can be explained in three interaction modes: (1) carboxyl groups of GO and amine groups of PEI-DTPA reacted and form amide bonding, (2) electrostatic interaction carboxyl groups

of GO and amine groups of PEI-DTPA, (3) hydrogen bonding between hydroxyl, carboxyl groups and primary amine.

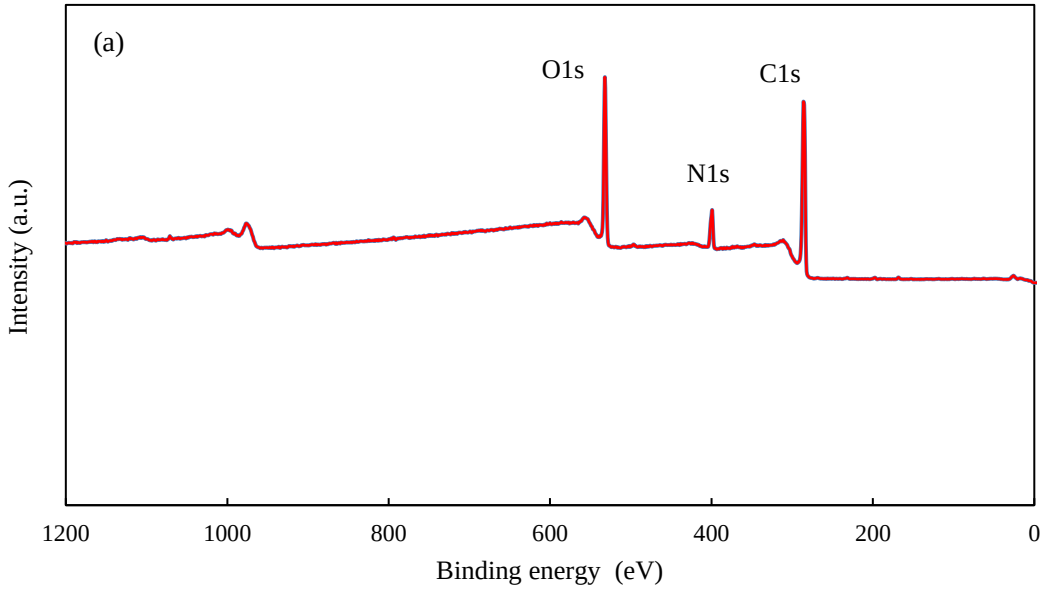

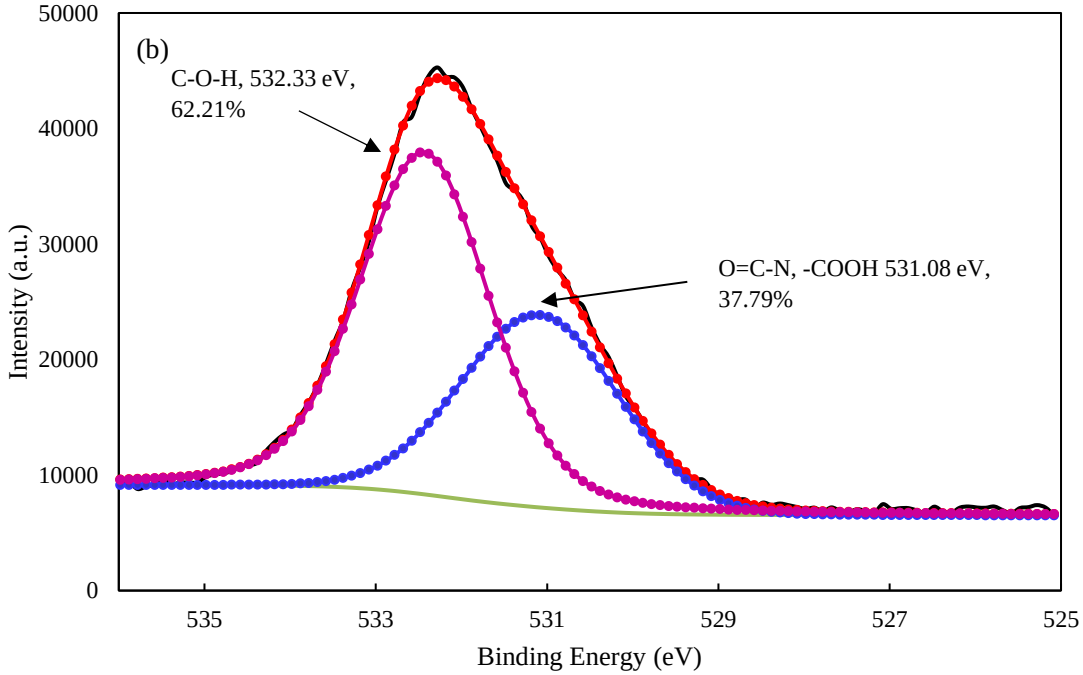

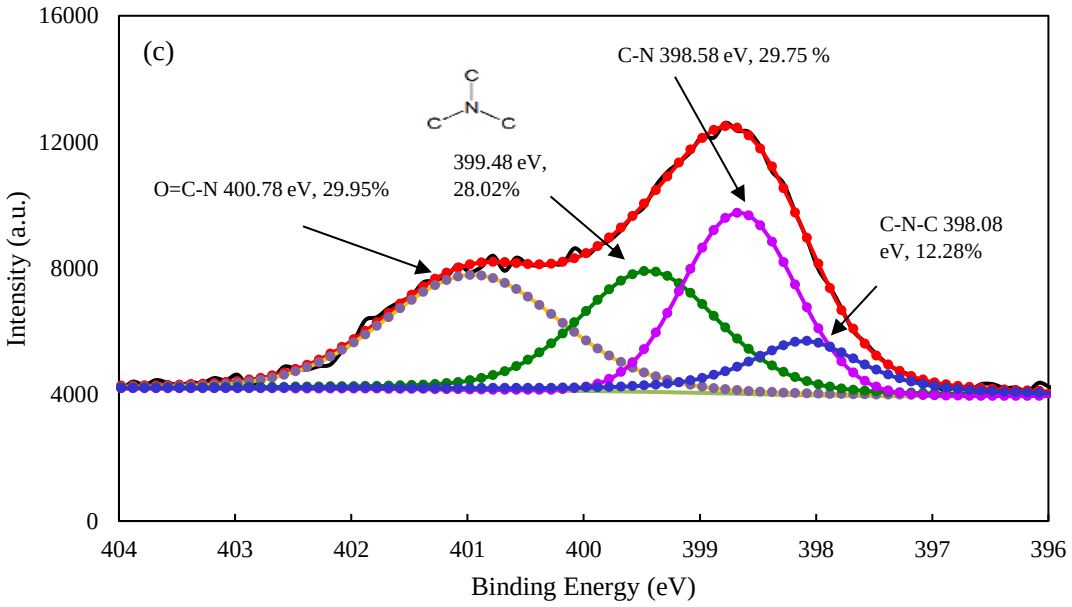

Figure 4. 5 (a) Wide scan XPS of RGO-(PEI-DTPA); (b) is deconvolved curve of O1s spectra of RGO-(PEI-DTPA); (c) is deconvolved curve of N1s of RGO-(PEI-DTPA).

Other characterization results such as surface area, porosity, zeta potential and elemental composition are summarized in Table 4.1 for GO, RGO-PEI, RGO-(PEI-DTPA). BET specific surface area for GO is 297.8 $m^2 g^{-1}$ and decreased to 250.8 $m^2 g^{-1}$ and 227.4 $m^2 g^{-1}$ for RGO-PEI and RGO-(PEI-DTPA) nanocomposites, respectively, after chemical modification. This could be due to the fact that some pores of GO nanosheets are blocked by attaching PEI or PEI-DTPA molecules. Zeta potential of each sample was measured in distilled water, which was lower for RGO-(PEI-DTPA) than that for RGO-DTPA due to the less amount of amino groups and higher amount of carboxylic acid groups from DTPA. Furthermore, the results from the elemental analyses of adsorbates and GO are presented in Table 4.1. Compared with GO, the presence of nitrogen in RGO-PEI and RGO-(PEI-DTPA) proved that adsorbents were successfully synthesized.

Table 4. 1 Characteristics of GO, RGO-PEI, RGO-(PEI-DTPA).

		GO	RGO-PEI	RGO-(PEI-DTPA)
BET surface area ($m^2 g^{-1}$)		297.8	250.8	227.4
Total pore volume ($cm^3 g^{-1}$)		2.97	2.42	2.31
Zeta potential (mV)		-39	11.8	6.4
Elemental composition (%)	C	44.41	57.83	55.67
	N	0.0	9.97	7.6
	H	0.59	5.11	2.05

Moreover, the amounts of carboxyl and amino groups on RGO-(PEI-DTPA) were measured using an acid-base titration method with 0.01 M HCl or 0.01 M NaOH. The amounts of amino groups and carboxyl groups were 4.75 mmol g^{-1}, 6.38 mmol g^{-1} respectively, confirming our results from elemental analysis.

The thermal stability of GO, RGO-PEI, RGO-(PEI-DTPA) nanocomposites was investigated by thermogravimetric analysis (TGA), and the findings are illustrated in Figure 4.6. The first weight loss for GO happened between 30°C and 100°C, which is

related to moisture loss which is around 15%. Decomposition of labile oxygen-containing functional groups of GO (approximately 22% weight loss) occurred between 100°C and 200°C. The weight losses for bulk pyrolysis of the carbon skeleton was below 600°C and accounted for about 10% [78]. The thermogravimetric analysis curve of RGO-(PEI-DTPA) shows the weight loss of 23% in the range of 30°C -250°C for the loss of adsorbed moisture and unstable oxygen groups. Decomposition of stable oxygen groups and polyimide (40% weight loss) happened at 250°C–600°C. Apparently, the weight loss of both synthetic nanocomposites was larger than GO nanosheets in the second stage, revealing the fact that some of GO groups bonded with PEI or PEI-DTPA molecules and therefore made it more difficult to decompose.

The weightlessness of GO, RGO-PEI, and RGO-(PEI-DTPA) were 44.63%, 67.24%, 49.94 % respectively. Thus, RGO-PEI and RGO-(PEI-DTPA) nanocomposites contained about 22.61%, 5.31% of PEI and PEI-DTPA respectively.

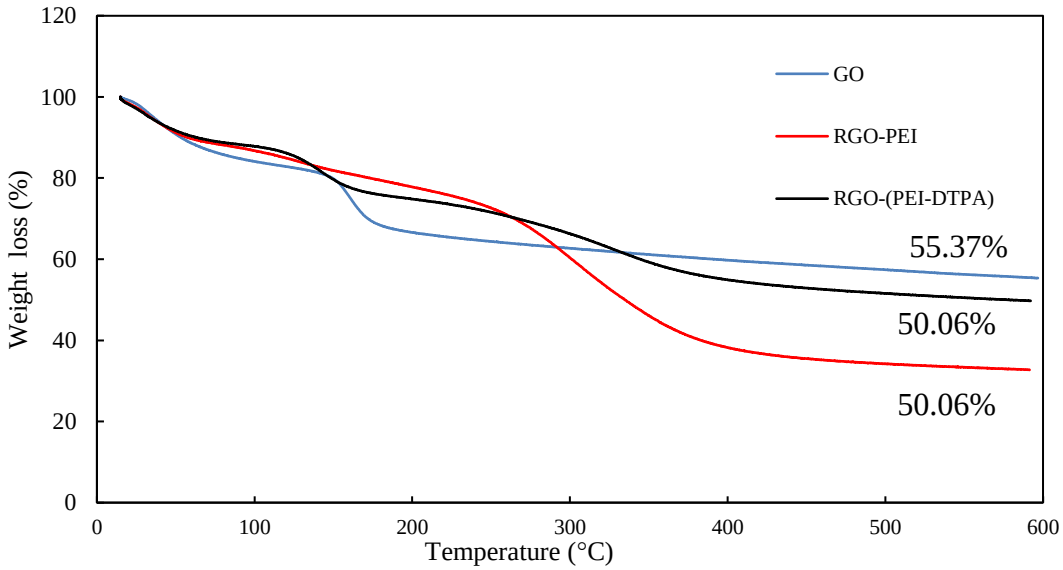

The SEM images of the GO, RGO-(PEI-DTPA) and Cr (VI) ion-loaded RGO-(PEI-DTPA) are shown in Figure 4.7. The GO represents the smooth surface and wrinkle edge and after modification with PEI-DTPA had a much rougher surface due to attaching PEI-DTPA (Figures 4.7 a and b). In addition, after reaction with Cr (VI), Pb (II), Cu (II) ions, the morphology of RGO-(PEI-DTPA) has been changed enormously, implying the heavy metal ions were loaded onto RGO-(PEI-DTPA) (Figures 4.7 c and d and e).

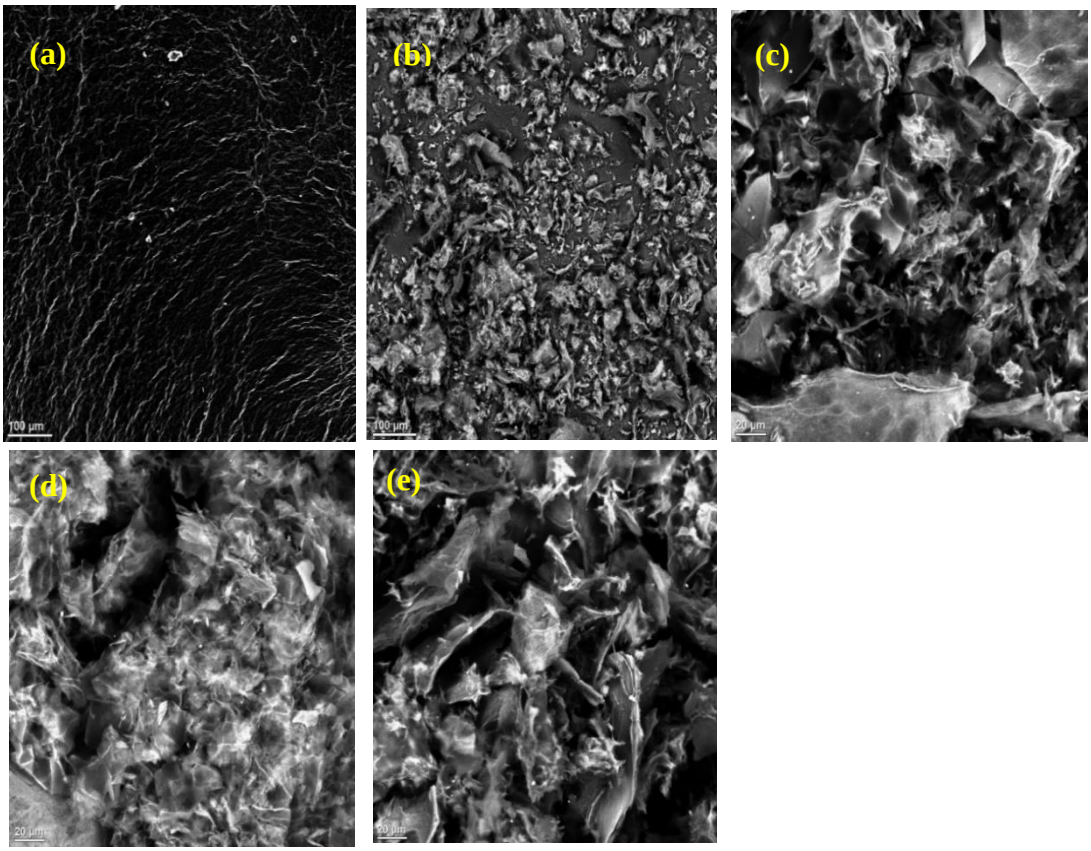

Figure 4. 7 SEM image of (a) GO, (b) RGO-(PEI-DTPA), (c) RGO-(PEI-DTPA) after adsorption of Cr (VI) (d) RGO-(PEI-DTPA) after adsorption of Pb (II), (e) RGO-(PEI-DTPA) after adsorption of Cu (II).

The EDS spectra after adsorption are also given in Figure 4.8 for three heavy metal ions sorption. As can be seen from Figure 4.8, the peaks of Cr (VI), Pb (II), Cu (II) are obvious, confirming the existence of each heavy metal ion on the surface of GO nanosheets after adsorption and further demonstrating that RGO-(PEI-DTPA) successfully removed heavy metal ions from solutions.

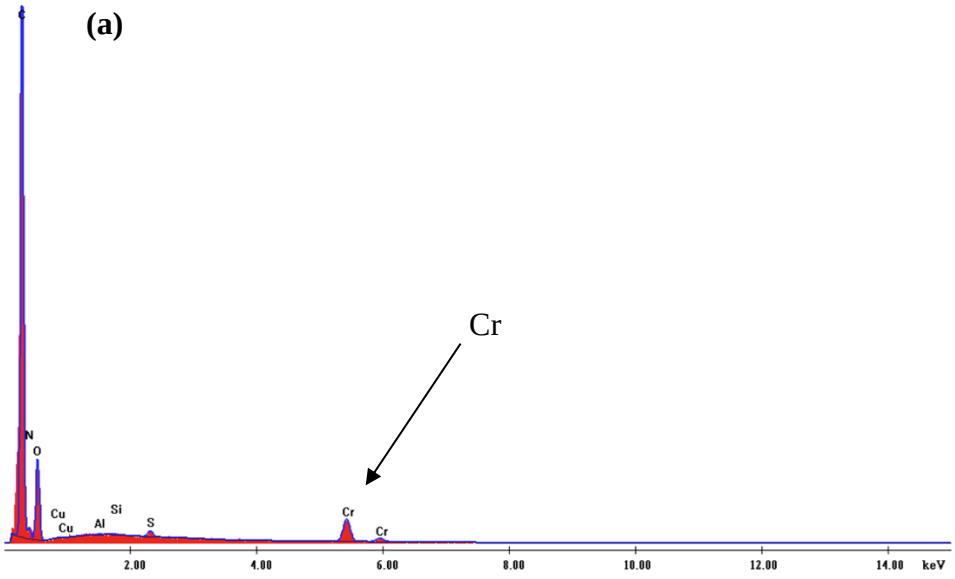

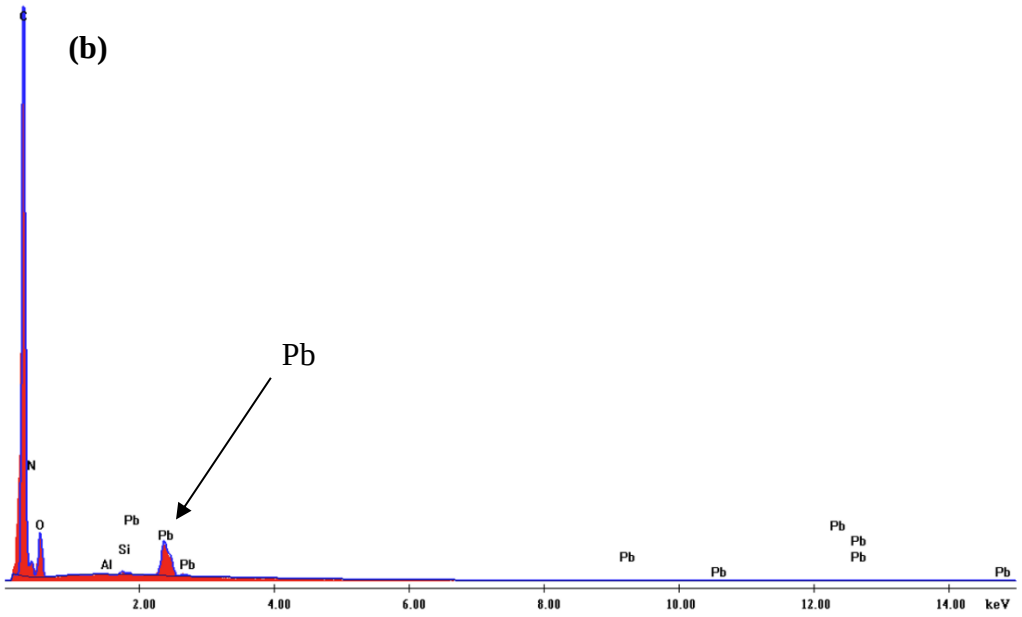
(b)
Pb
C
N
O
Al
Si
Pb
Pb
Pb
Pb
Pb
Pb
Pb
Pb
Pb
2.00
4.00
6.00
8.00
10.00
12.00
14.00
keV

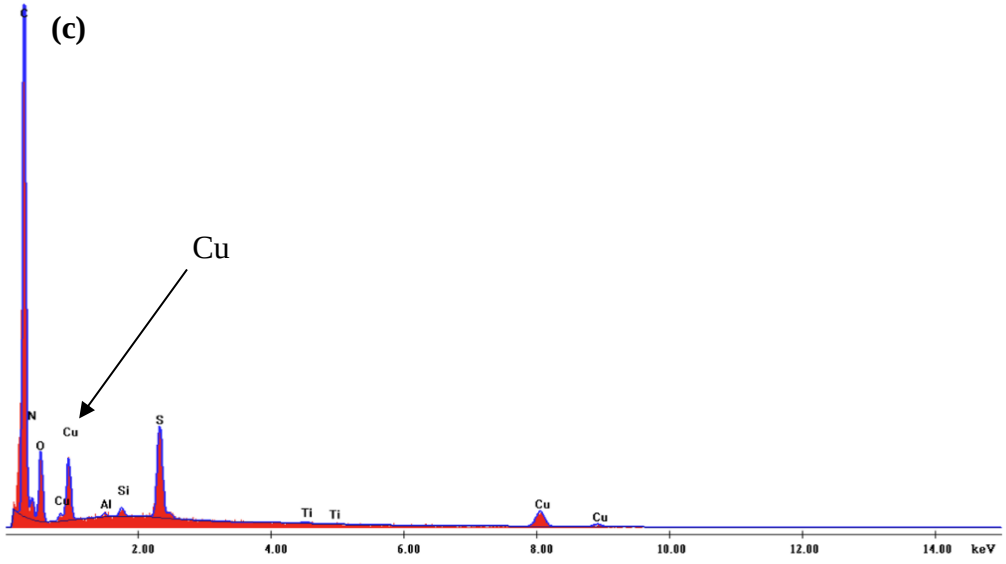
(c)
Cu
C
N
O
Cu
Cu
Al
Si
S
Ti
Ti
Cu
Cu
2.00
4.00
6.00
8.00
10.00
12.00
14.00
keV

Figure 4. 8 EDS spectra of (a) RGO-(PEI-DTPA) after adsorption of Cr (VI) (b) RGO-(PEI-DTPA) after adsorption of Pb (II), (c) RGO-(PEI-DTPA) after adsorption of Cu (II).

4.3 Adsorption studies

4.3.1 Adsorption behavior

In this study, two oppositely charged metal ions (Cu (II), Pb (II)) and Cr (IV) were used for the adsorption evaluation of RGO-PEI, RGO-(PEI-DTPA) nanocomposites. In an aqueous solution, Cr (VI) could be available as different species depending on pH. When pH is less than 1, the main species is H_2CrO_4; at pH between 2 and 6, $HCrO_4^-$ and the $Cr_2O_7^{2-}$ are in equilibrium and at pH above 6, Cr (VI) forms CrO_4^{2-} (Figure 4.9 a). On the other hand, cationic heavy metal ions Pb (II), Cu (II) at pH below 7 are mostly in cationic form and when pH reaches above 7 different forms of metal hydroxide (as shown in Figures 4.9 b and c) precipitate in aqueous solution. The experiments in this study were not done above that pH because of possible precipitated heavy metals that might interfere with the adsorption sites.

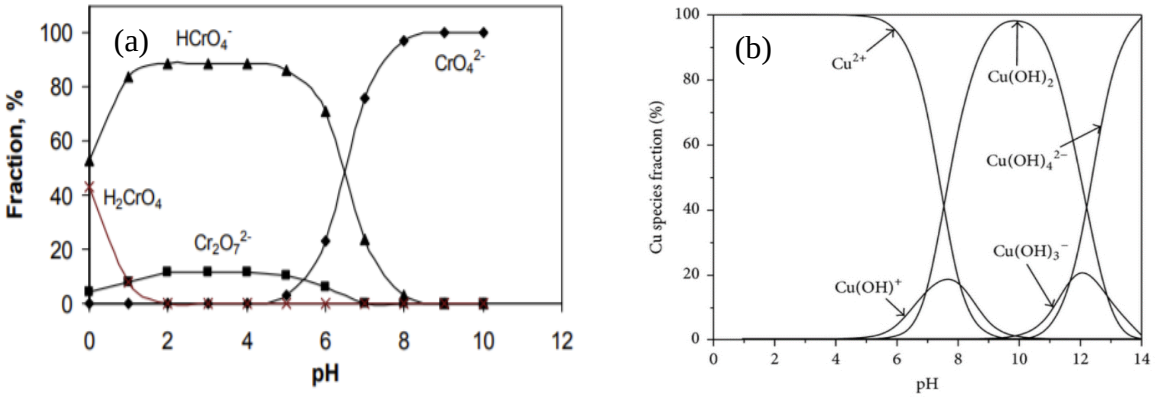

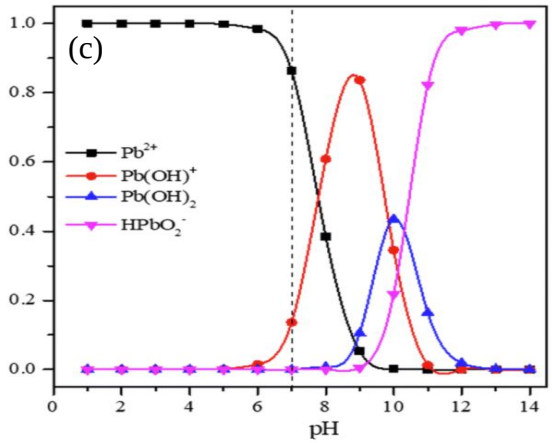

Figure 4. 9 (a) Relative distribution of Cr (VI) species as a function of pH, (b) Relative distribution of Cu (II) species as a function of pH, (c) Relative distribution of Pb (II) species as a function of pH [86-88].

4.3.2 Effect of pH

pH is an essential parameter for determining the surface charge of the adsorbent as well as the metal ion in the solution and consequently the removal efficiency of heavy metal ions from an aqueous solution will be impacted [89]. The effect of pH on the remaining concentration after adsorption of RGO-(PEI-DTPA) for Cr (VI), Cu (II) and Pb (II) is shown in Figures 4.10 a and b.

As can be seen, the adsorption removal of Pb (II) and Cu (II) increased slightly with the rise of pH values and this could be explained by the fact that at acidic pH, hydrogen ions compete for the adsorption sites. The experiment did not conduct at values above 8 because of hydroxide precipitate formation of metal ions as $Cu(OH)_2$ and $Pb(OH)_2$ [90]. For Cr (VI) solution, the situation is different since chromium ions could be found in various forms depending on pH of a solution. $HCrO_4$ and Cr_2O_7 exist at the pH range of 2 to 6 and these negative ions ($HCrO_4$ and Cr_2O_7) were immobilized to the protonated amino groups in

RGO-(PEI-DTPA) via electrostatic attraction at acidic pH [91]. The removal rate was almost the same at different PH for Cr (VI) removal.

It can be concluded that RGO-(PEI-DTPA) nanocomposite has a broad range of pH application for Cr (VI), Cu (II) and Pb (II) adsorption.

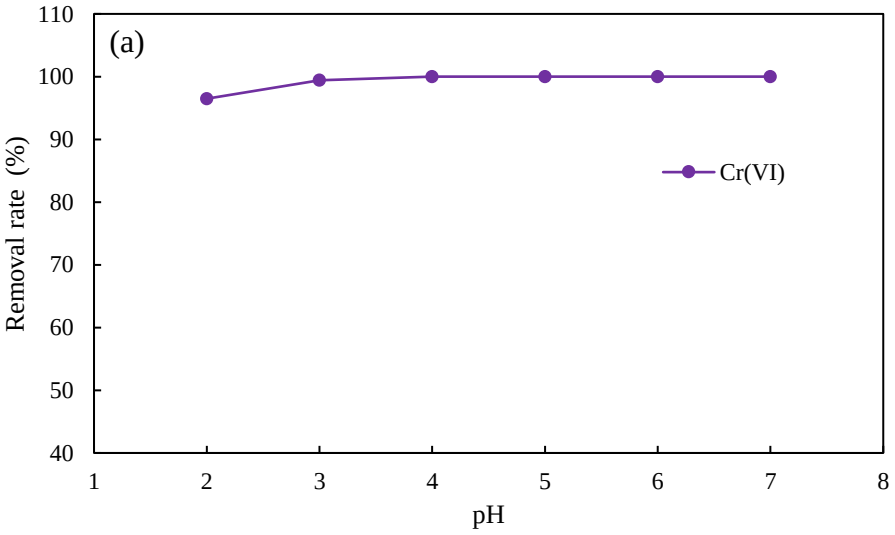

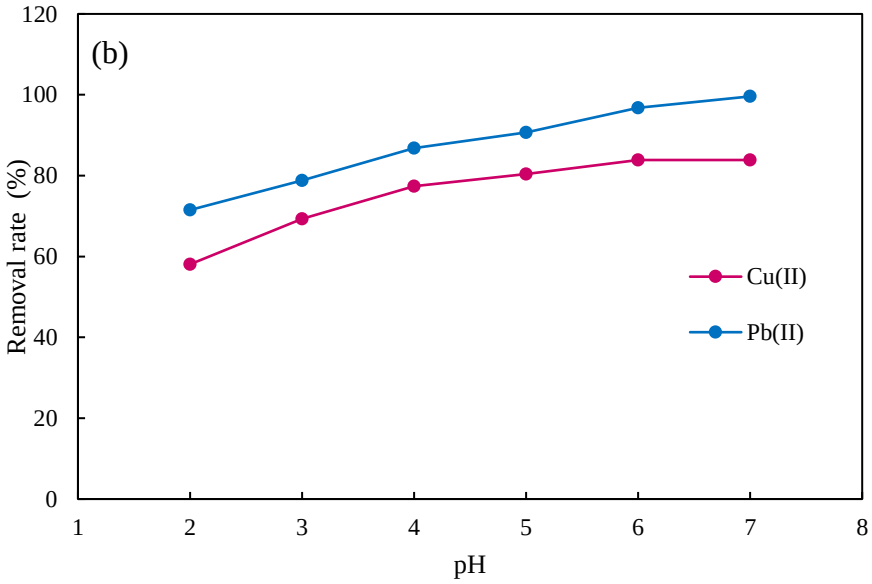

Figure 4. 10 Effect of different pH on the removal rate of RGO-(PEI-DTPA) for (a) Cr (VI), (b) Cu (II), Pb (II).

(Concentration of each heavy metal ion: 3 mg L^{-1}, adsorbent dosage 1g L^{-1}, room temperature, time of contact 5 h).

4.3.3 The effect of the adsorbent dosage

The effect of the adsorbent dosage RGO-(PEI-DTPA) on the removal ratio of Cr (VI) was investigated by adding different amounts of RGO-(PEI-DTPA) to 50 ml of Cr (VI) ion concentration (3mg L^{-1}) at room temperature with stirring speed 150 rpm and contact time 5h. The results in Figure 4.11 showed that with increasing the adsorbent dose, the removal rate of Cr (VI) increased sharply from 52% to 91 % and this is due to more adsorptive sites that could be effectively employed for Cr (VI) removal. When the adsorbent was 1 g L^{-1}, the removal rate reached 100% ; thus 1 g L^{-1} was selected as the optimum dose for subsequent experiments.

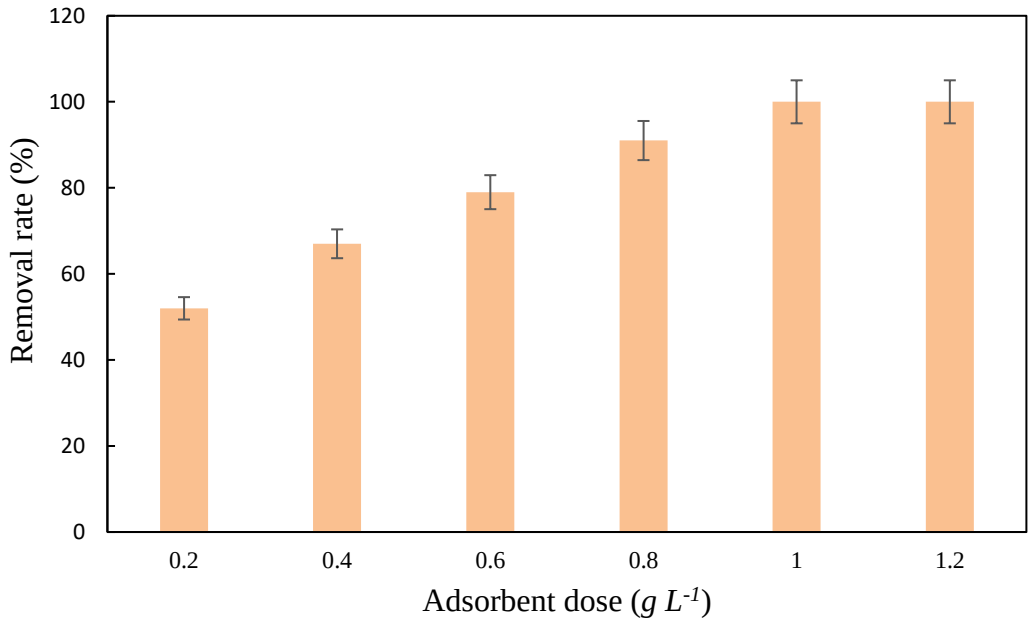

Figure 4. 11The effect of the adsorbent dose RGO-(PEI-DTPA) on the removal efficiency of Cr (VI).

(Concentration of each heavy metal ion: 3 mg L^{-1}, pH 7, room temperature, time of contact 5 h).

4.3.4 Adsorption kinetics

The impacts of time on the adsorption efficiency of RGO-PEI and RGO-(PEI-DTPA) was investigated and shown in Figures 4.12 and 4.13 and 4.14. The study was conducted at initial concentrations of 2 mg L^{-1}, 3.1 mg L^{-1}, 3 mg L^{-1} from 50 mL of Pb (II), Cu (II), Cr (VI) solutions respectively. For this experiment, the temperature was 25°C, pH 7, solid adsorbent was 1 g L^{-1}.

Starting concentration of Pb (II) in solution was 2 mg L^{-1} for both nanocomposites in solution and the remaining concentration for RGO-PEI adsorbent even after 5 h did not reach the level of the safe drinking standard (US EPA) which is 0.01 mg L^{-1} (Figures 4.12 a and b). On the contrary, in the same experimental condition, Pb (II) concentration in RGO-(PEI-DTPA) nanocomposite solution only after 20 minutes reached below 0.01 mg/L. This observation is related to available carboxylic acid groups from DTPA molecule on RGO-(PEI-DTPA) nanocomposite compared to RGO-PEI nanocomposite that adsorbed Pb (II) preferentially.

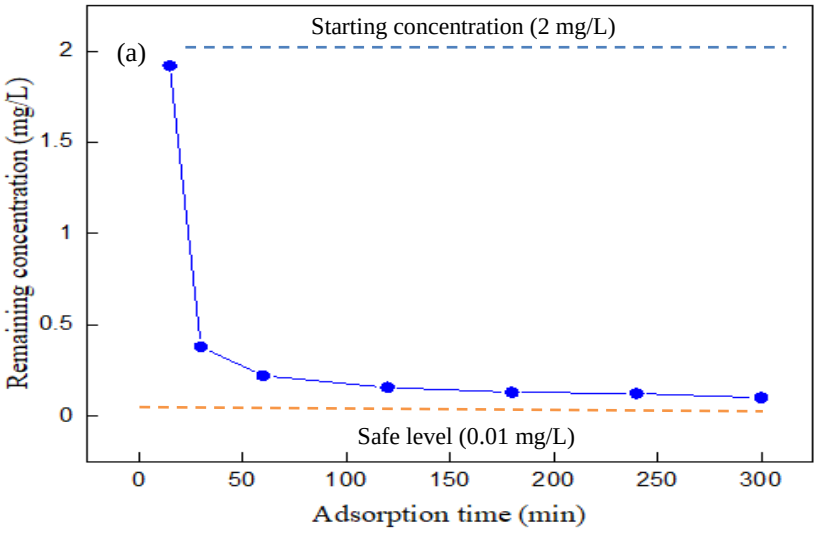

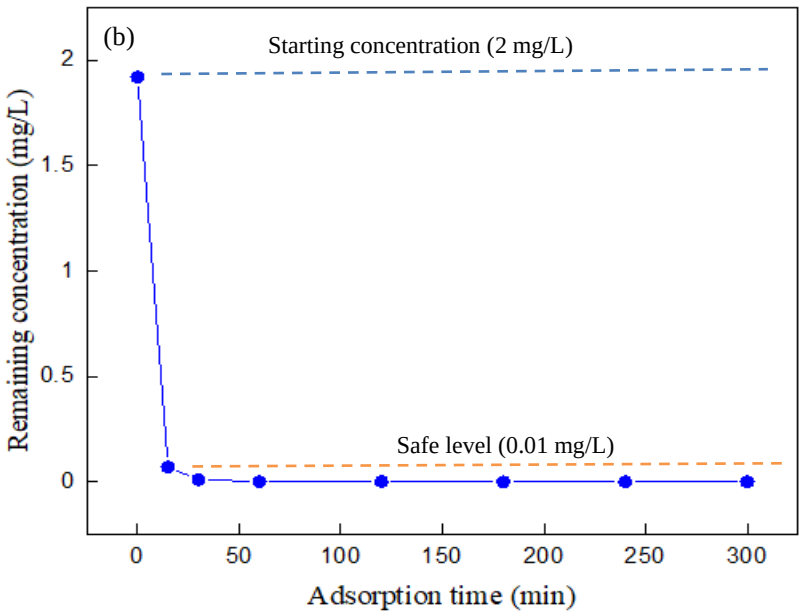

Figure 4. 12(a, b) effects of adsorption time on the remaining concentration after adsorption of RGO-PEI and RGO-(PEI-DTPA) for Pb (II) solution.

In the case of Cu (II) solution, when starting concentration was 3.1 mg L^{-1}, both RGO-PEI and RGO-(PEI-DTPA) nanocomposites adsorbents could successfully adsorb Cu (II) to below 2 mg L^{-1} which is a safe level of the safe drinking standard (US EPA). However, RGO-(PEI-DTPA) nanocomposite can reduce the concentration to 0.5 mg L^{-1}, whereas the remaining concentration in RGO-PEI nanocomposite reached only 1.6 mg L^{-1} (Figures 4.13 a and b). Again, this is correlated to more available adsorptive sites such as carboxylic acid groups that come from DTPA molecules on RGO-(PEI-DTPA) surface.

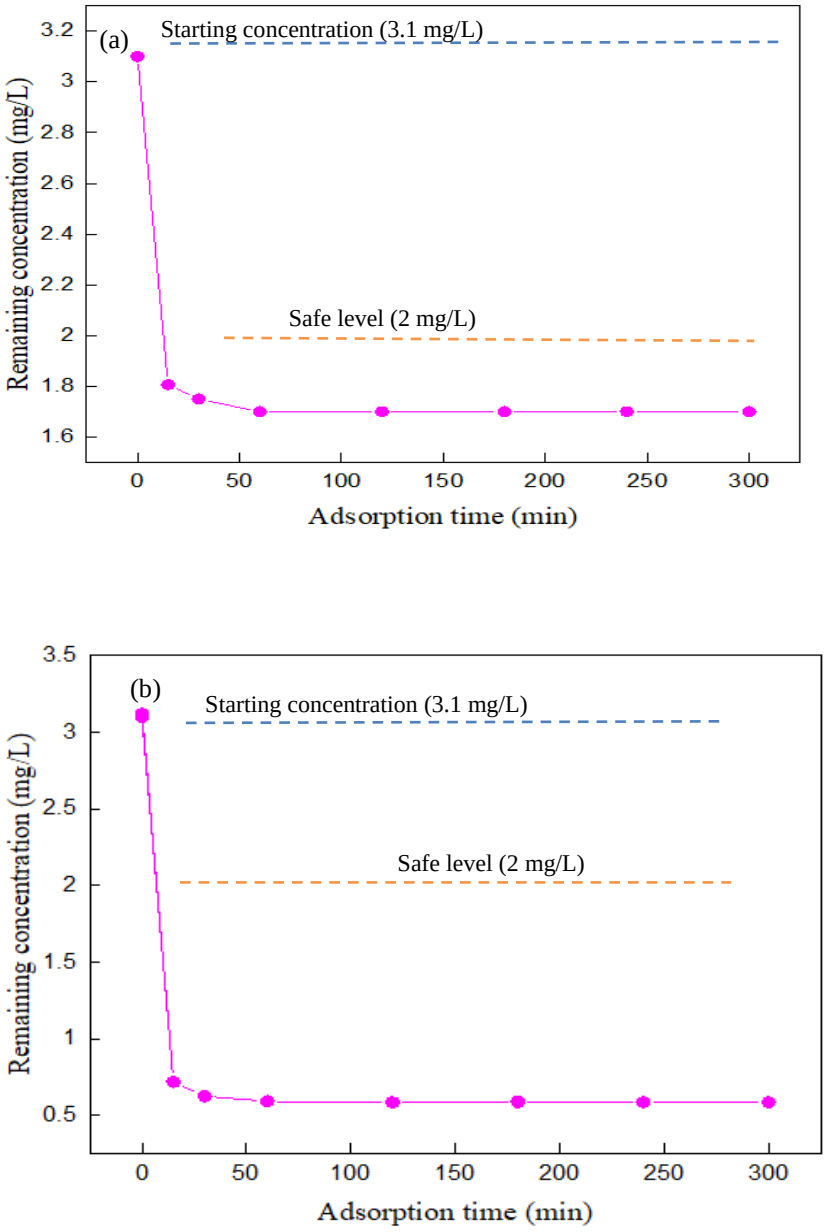

Figure 4. 13 (a, b) effects of adsorption time on the remaining concentration after adsorption of RGO-PEI and RGO-(PEI-DTPA) for Cu (II).

RGO-PEI and RGO-(PEI-DTPA) nanocomposites were also examined for Cr (VI) removal and exhibited excellent performance. When the initial concentration of Cr (VI) was 3 mg L^{-1}, RGO-PEI completely removed Cr (VI) from the solution after 120 min and reached the safe level of drinking water. For RGO-(PEI-DTPA) nanocomposite, at the same experimental condition, the remaining concentration of Cr (VI) reached the safe level after 165 min which might be related to less available amino groups on RGO-(PEI-DTPA) sheets, which was confirmed from elemental analysis results. The results for Cr (VI) adsorption are shown in Figures 4.14 a and b.

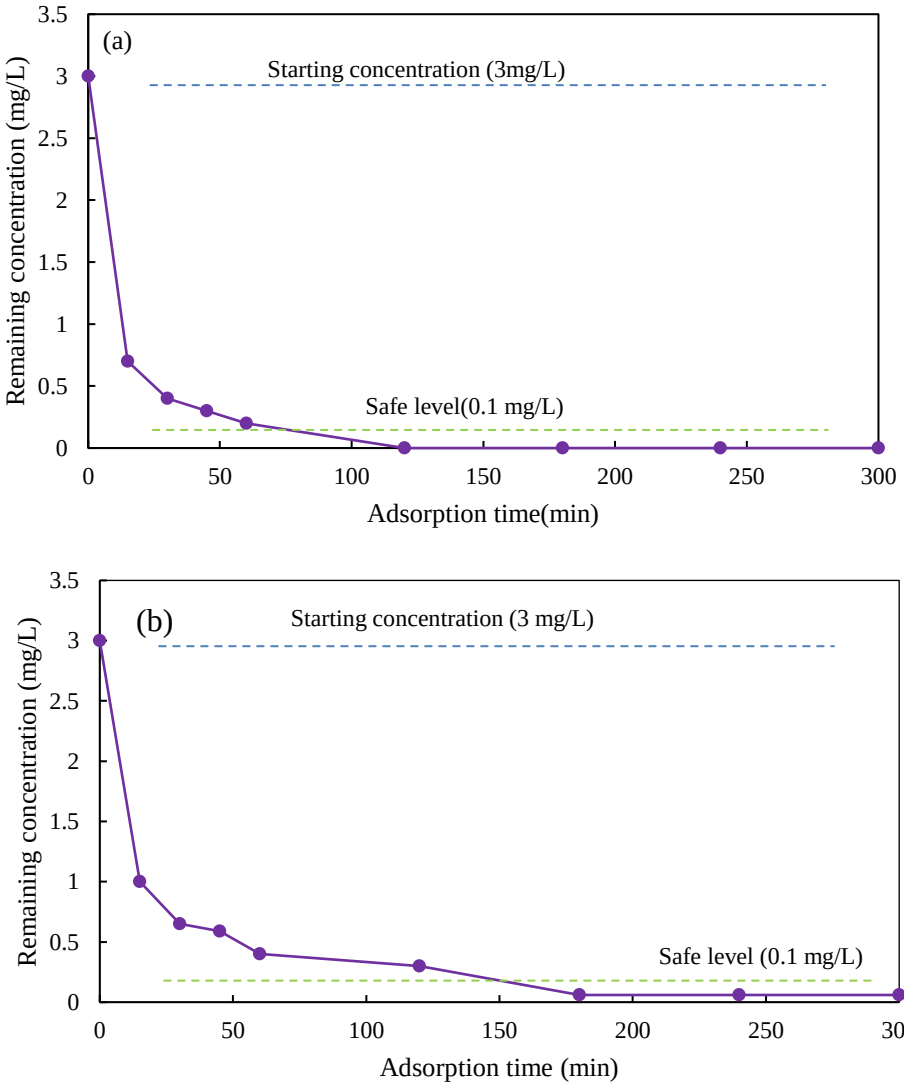

Figure 4. 14(a, b) effects of adsorption time on the remaining concentration after adsorption of RGO-PEI and RGO-(PEI-DTPA) for Cr (VI) respectively.

Competitive adsorptions of Cr (VI), Cu (II) and Pb (II) on RGO-(PEI-DTPA) were also done and the results are shown in Figure 4.15. In the mixture of Pb (II) and Cu (II) heavy metal ions, 82.75% of Pb (II) adsorbed on the surface of RGO-(PEI-DTPA), while this number for Cu (II) is only 17.25%. It can be interpreted that synthetic absorbent had a higher affinity towards Pb (II) than Cu (II) which is in agreement with our previous results showing higher removal rate for Pb (II) compared to Cu (II) (Figures 4.12 and 4.13). Furthermore, the same experiment was done in the mixture of Pb (II), Cr (VI) solution and the results demonstrated 54% of Cr (VI) adsorbed compared to 46% of Pb (II).

The obtained results illustrated that the higher removal was accomplished in the order of Cr (VI) > Pb (II) > Cu (II) and revealed the fact that the amino groups have a stronger affinity to anion Cr (VI) than cations (Pb (II), Cu (II)). At the same time, carboxyl groups contributed more to interact with cations. Clearly, RGO-(PEI-DTPA) nanocomposite with a high density of amino and carboxyl and hydroxyl groups acted as excellent adsorbent to remove low-level cationic and anionic heavy metal ions (Pb (II), Cu (II), Cr (VI)) through cooperation mechanism.

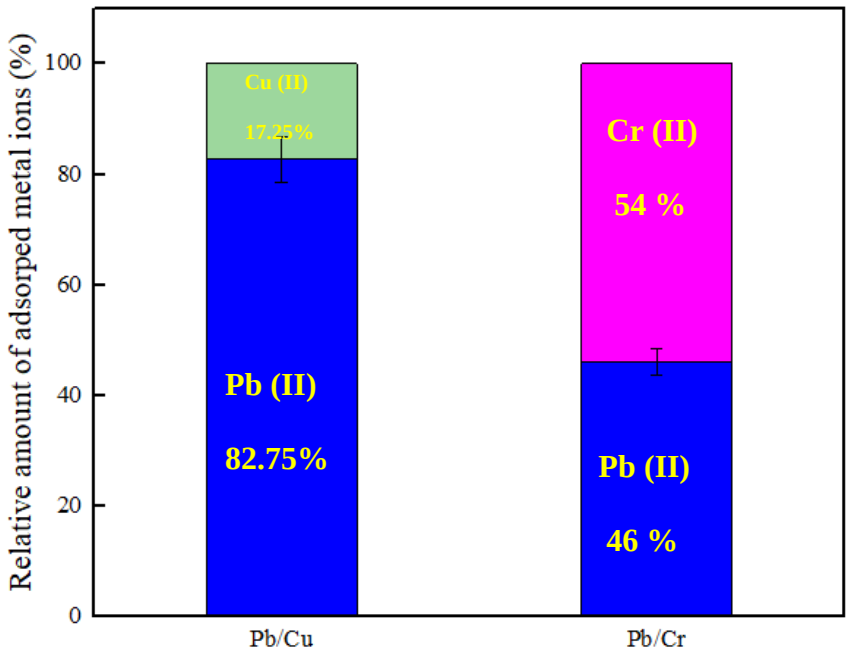

Figure 4. 15The binary competitive adsorption of RGO-(PEI-DTPA).

(Concentration of each heavy metal ion: 5 mg L^{-1}, pH 7, room temperature, time of contact 5 h).

The adsorption mechanism for anionic metal ions such as Cr (VI) is summarized as follows. In an acidic environment (pH < 7), the amino groups of RGO-PEI or RGO-(PEI-DTPA) nanocomposites were positively charged and in this way, the negatively charged CrO_4^{2-}, $Cr_2O_7^{2-}$ and $HCrO^{4-}$ adsorbed electrostatically on each nanocomposite [92].

Moreover, nitrogen atoms in amino groups have a lone pair of electrons that could chelate with an empty orbital of Cr (VI). Another theory is that Cr (VI) is converted to non-toxic Cr (III) by a redox reaction and nitrogen and oxygen atoms are chelated with both Cr (VI) and Cr (III) ions [93]. The adsorption mechanism of Cr (VI) on RGO-PEI or RGO-(PEI-DTPA) nanocomposites was proposed to involve multiple interactions including chelating reactions, electrostatic reactions and oxidation-reduction reactions. This excellent

adsorption capacity for Cr (VI) comes from high density of amino groups of each nanocomposite. The adsorption mechanism for cationic metal ions (Pb (II), Cu (II)) is summarized in this way: the carboxyl groups dominated the adsorption sites and chelated with Pb (II) and Cu (II) ions. Besides, attaching PEI or PEI-DTPA on GO nanosheets prevented the aggregation due to π-π stacking of GO aromatic ring; and as a result, more active sites would be available.

Thus, the adsorption mechanism of RGO-(PEI-DTPA) nanocomposites for removing low-level heavy metal ions was associated with both amino and carboxyl groups via cooperation mechanism.

The impacts of exposure time on the sorption efficiency of RGO-(PEI-DTPA) for Cr (VI), Pb (II), Cu (II) ions in solution were examined and results are presented in Figures 4.16 a and b and c respectively. At the beginning of the experiment (within the first 50 min), the adsorption proceeded very fast and that is because of a higher number of active sites on RGO-(PEI-DTPA) surface. However, the available adsorption sites become less with more heavy metal ion adsorption leading to a slower adsorption rate. This slower rate might be correlated to several factors such as fewer number of available adsorption active sites, electrostatic repulsion between captured heavy metal ions and incoming ions. Several studies reported a two-phase pattern in the adsorption in which in the second phase the occupation of available active sites occurred at slower rate than beginning because of a low number of sites for adsorption [94, 95].

The experimental data from RGO-(PEI-DTAP) nanocomposite were fitted to two well-known kinetics models namely pseudo-first-order (PFO) and pseudo-second-order (PSO) (Figure 4.16).

The parameters of PFO and PSO kinetic models (q_e, K_1, K_2) with their corresponding error function (R^2) are shown in Table 4.2. In this study, non-linear regression was used to examine how experimental data fit to these models' parameters and this optimization needs to be done by comparing the error function (R^2).

It is concluded that PSO kinetic model is better fitting for all heavy metal ions removal according to higher R^2 values obtained from Figure 4.16. Moreover, calculated q_e from PSO model is much closer to obtained experimental results of heavy metal ion adsorption on RGO-(PEI-DTPA).

The primary assumption of PSO kinetic model is that chemical sorption may be the rate-limiting steps that happen through sharing electrons between metal ions and adsorbent [96].

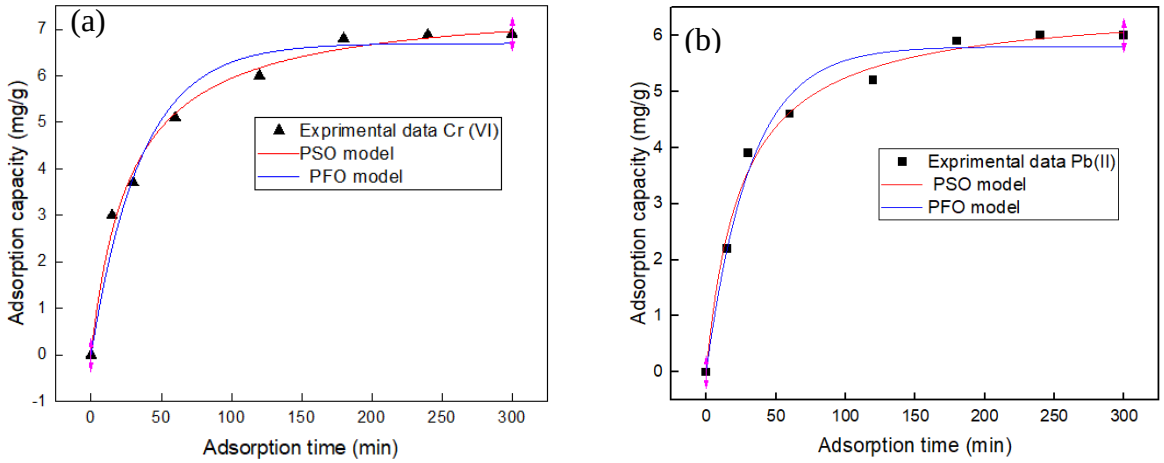

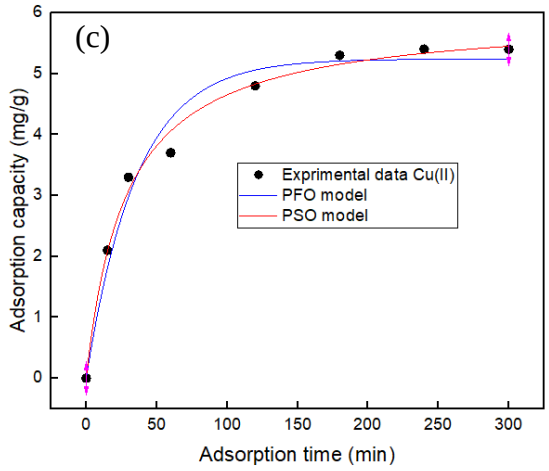

Figure 4. 16 (a,b,c) Pseudo-first-order and pseudo-second-order nonlinear fitting for Cr (VI),Pb (II), Cu (II) adsorption onto RGO-(PEI-DTPA) (pH 7, concentration of each heavy metal ion: 10 mg L^{-1}, adsorbent dosage 1 g L^{-1}, room temperature, time of contact 5 h).

Table 4. 2 kinetic adsorption parameters onto RGO-(PEI-DTPA)

Model	Parameters	Cu^{2+}	Pb^{2+}	Cr^{6+}
PFO model	$K_1(min^{-1})$	0.02796	0.316	0.02801
	q_e (mg g^{-1})	5.24115	5.80016	6.6946
	R^2	0.97525	0.9831	0.97742

PSO model	K_2 (g mg^{-1} min^{-1})	0.00596	0.00606	0.00472
	q_e (mg g^{-1})	5.96921	6.56437	7.5996
	R^2	0.992	0.99223	0.9936

4.3.5 Adsorption Isotherm Models

Equilibrium experiments with linear fit were undertaken for the loading of Cu (II), Pb (II), Cr (VI) ions onto RGO-(PEI-DTPA) to obtain Langmuir and Freundlich isotherms (Figures 4.17 a and b). The experimental conditions were explained in section 3.4.2., and metal ions uptake by RGO-(PEI-DTPA) was determined.

Similar to applied kinetic models, this method determines isotherm model parameters by ensuring that the deviation of the coefficients obtained from isotherm modeling results and experimental data is minimum.

As explained before, Langmuir isotherm is utilized for describing the monolayer adsorption on the uniform binding sites on the surface with equivalent adsorption energies, whereas Freundlich model describing the adsorption on the uneven surface with an exponential distribution of active sites across the adsorbent.

All the relevant data from the plots of the isotherms based on these two models are presented in Table 4.3 and the values of correlation coefficient show the goodness of a fit for our system.

The higher values of correlation coefficient suggest that model better fit the data from the experiment.

It is resulted that Langmuir model describes the sorption of Cu (II) and Pb (II) from an aqueous solution onto RGO-(PEI-DTPA) better than the other model due to higher R^2 values. However, for Cr (VI) adsorption data fitted better into Freundlich model. This behavior mostly happens when the maximum coverage has not been attained, e.g., in dilute systems and/or when the adsorption capacity of adsorbent is too high and for our studied system it is because of low studied concentration.

The energy constant "K_L" in Langmuir equation relates to the heat of adsorption and the values for Cu (II), Pb (II) were 0.82 and 0.13 for Cu (II) and Pb (II) respectively. This indicates that Pb (II) ions uptake onto the surface of the RGO-(PEI-DTPA) has a comparatively lower heat of adsorption. Moreover, the calculated R_L parameter from equation 3.6 for all heavy metal ions is between 0 and 1 and $K_L > 0$; therefore it could be concluded that Cr (VI), Cu (II), Pb (II) adsorption was favorable. The maximum calculated adsorption capacities for Cu (VI), Pb (II), Cr (II) were 5.14 mg g^{-1}, 16.31 mg g^{-1}, 8.53 mg g^{-1} respectively from Langmuir equation.

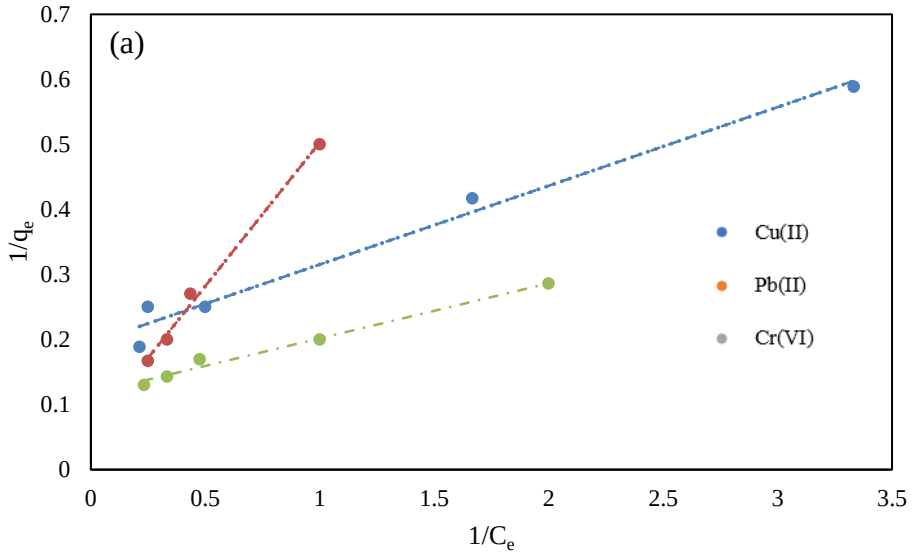

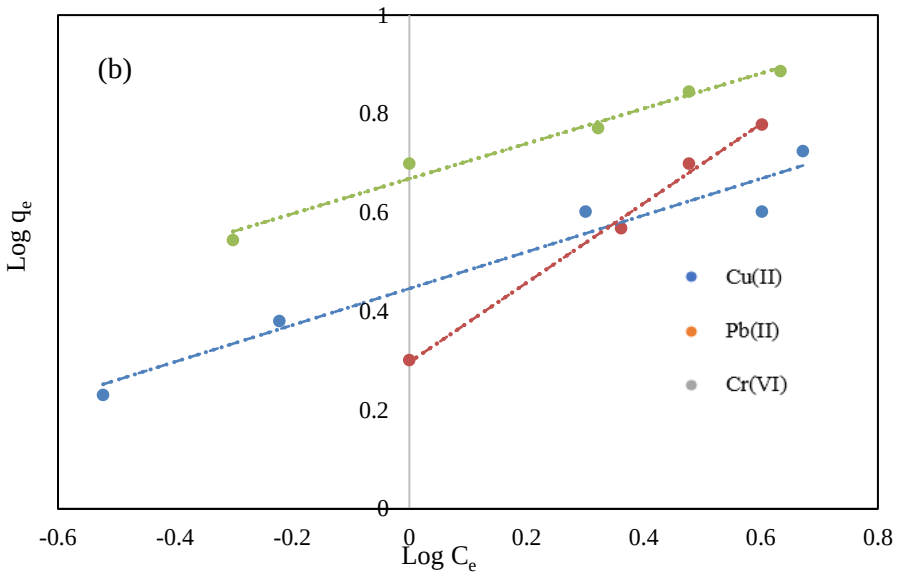

Figure 4. 17 Langmuir (a) and Freundlich (b) isotherms for the adsorption of Cu (II), Pb (II), and Cr (VI) ions on RGO-(PEI-DTPA).

Table 4. 3Parameters for the Langmuir and Freundlich models of Cu (II), Pb (II), and Cr (VI) ions on RGO-(PEI-DTPA).

Model	Parameters	Cu^{2+}	Pb^{2+}	Cr^{6+}
Langmuir isotherm	q_m (mg g^{-1})	5.1413	16.3132	8.5324
	K_L (L mg^{-1})	0.8264	0.1387	1.3853
	R^2	0.9868	0.9943	0.9796

Freundlich isotherm	K_F (mg g^{-1})(L mg^{-1})$^{1/n}$	2.7938	1.9815	4.6633
	n	2.6968	1.2440	2.8169
	R^2	0.9488	0.9941	0.9797

4.3.6 Adsorption behaviour at high-level Cr (VI), Cu (II) and Pb (II) for RGO-PEI and RGO-(PEI-DTPA)

This experiment was done in order to evaluate the adsorption removal of both synthetic nanocomposites at higher heavy metal ion concentrations (Cr (VI), Cu (II), Pb (II)). When the initial concentration of each heavy metal ion was 100 mg/L, the results revealed that the affinities of the heavy metal ions toward adsorbents followed the order of Cr (VI) > Pb (II) > Cu (II) and showed in Figure 4.18. It could be concluded that the amino groups had a stronger affinity to anion Cr (VI) than cations (Cu (II), Pb (II)). Moreover, the removal rate of Cr (VI) was higher for RGO-PEI due to higher number of amino groups, whereas for Pb (II), Cu (II) the numbers were higher for RGO-(PEI-DTPA) because of oxygen adsorptive active sites (room temperature, pH 7, adsorbent 1 g L^{-1}).

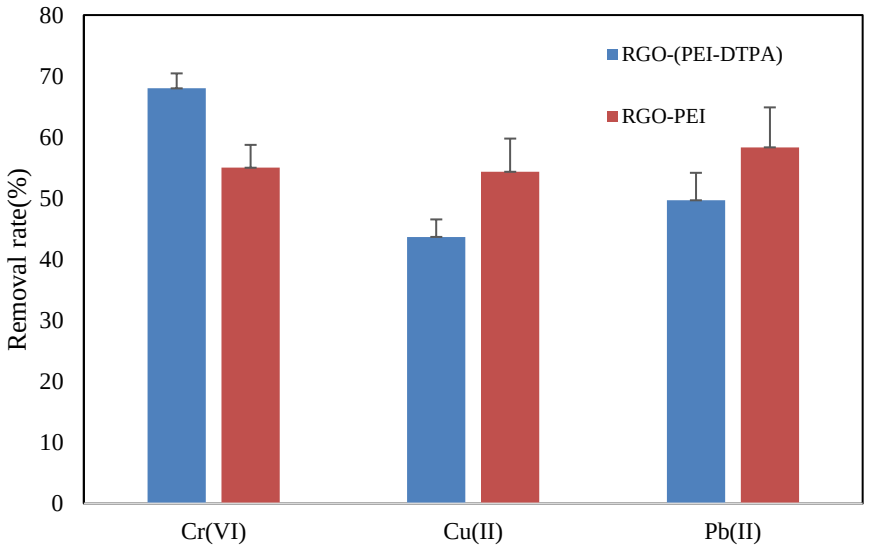

Figure 4. 18 The Removal rate of RGO-(PEI-DTPA) and RGO-PEI nanocomposites at high concentrations.

4.3.7 Regeneration of adsorbents

The reusability is important for adsorbents used in the practical treatment of wastewater to improve the cost-effectiveness. Desorption experiments with different resorptive solvents were reported for the regeneration of adsorbents; and then consecutive cycles of adsorption-desorption processes were conducted multiple times to evaluate reusability. In order to evaluate the long-term usability of synthetic adsorbents, multiple regeneration experiments were performed via adsorption-desorption cycles at 25 ˚C. In the adsorption process, heavy metal-loaded adsorbent (1 mg L^{-1}) was prepared from a heavy metal ion solution concentration of 3 mg L^{-1} at Ph 7 and contact time of 5 h.

For the desorption experiment, the prepared heavy metal-loaded RGO-(PEI-DTPA) adsorbents were desorbed using 0.1 mol of HCl and then NaOH solutions with a solid concentration at 1 g L^{-1} for 1 h.

The experimental results are shown in Figure 4.19 and the removal rate for RGO-(PEI-DTPA) nanocomposite even after 6 cycles is higher than 80% for Cr (VI) and Pb (II). Removal rate for Cu (II), Pb (II), Cr (VI) reached 77%, 80 %, 88% after 6 times. The decrease in the removal rate might be due to the fact that the acid caused damage during regeneration could result in losing adsorption sites on nanocomposite. However, the removal rates after 6 cycles were still satisfactory; with over 75% removal efficiency for each heavy metal ion. These results demonstrated that RGO-(PEI-DTPA) nanocomposite is a renewable adsorbent for lead, copper, chromium contaminated water treatment.

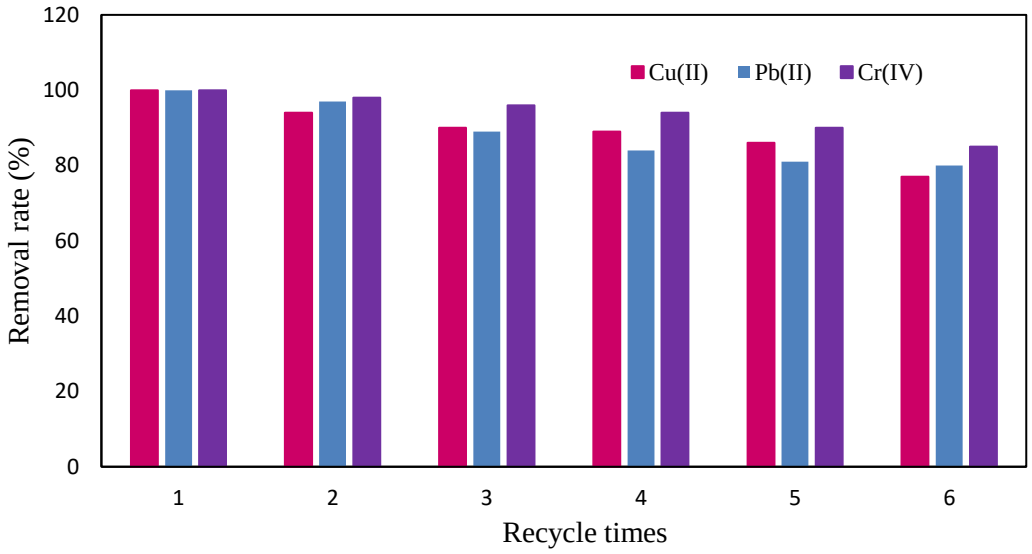

Figure 4. 19 Regeneration performance of RGO-(PEI-DTPA).

Chapter 5

Conclusions and Recommendations

5.1 Summary

Novel graphene oxide-based adsorbents (RGO-PEI, RGO-(PEI-DTPA)) with a high density of multiple active adsorption sites (amino groups, carboxyl groups) were successfully prepared using a facile chemical method. The structure of resultant adsorbents was well-characterized with different techniques such as FTIR, XPS, XRD.The removal rate of RGO-(PEI-DTPA) for Pb (II) 2 mg L^{-1}, Cu (II) 3 mg L^{-1} and Cr (VI) 3 mg L^{-1} reached 99 %, 83 % and 99 %, respectively, and the remaining concentration after adsorption reached the US EPA standards for Pb (II) and Cu (II) and Cr (VI), which is one of the main contributions from this study.

The structural and mechanistic studies indicated that the O atoms were the dominant adsorption sites for the adsorption of RGO-(PEI-DTPA) for cationic heavy metal ions Cu (II) and Pb (II), and N atoms were the dominant adsorption sites for the anion heavy metal ion Cr (VI). The results revealed that RGO-(PEI-DTPA) is of great potential for completely removing anionic and cationic heavy metal ions via a cooperation mechanism in low-concentration heavy metal ions environments.

The kinetic modeling indicates that the process of adsorbing Pb (II), Cr (VI), Cu (II) ions onto RGO-(PEI-DTPA) follows a pseudo-second-order (PSO) kinetics model, i.e., the adsorption is mainly governed by chemisorption. The isotherm studies showed that the adsorption of Pb (II) and Cu (II) is best described by Langmuir model whereas the

adsorption of the Cr (VI) is best characterized by Freundlich model. In addition, synthetic GO-based adsorbent exhibited good reusability.

5.2 Recommendations for future work

1) One of the technical challenges that need to be addressed before successfully realizing the practical applications of graphene oxide nanocomposites is to understanding the adsorption behavior of the nanocomposite adsorbents in actual wastewater containing multiple contaminants. Future research should be focused on competitive adsorption and their possible interference from other contaminants to target specific pollutant.

2) More research should be focused on enhancing the selectivity of adsorption and convenient separation of graphene oxide nanocomposites from the water after adsorption. Such studies are crucial for designing a practical adsorption system for the treatment of real industrial effluents.

3) There are many reports on batch adsorption graphene oxide nanocomposites, whereas treatment of real wastewaters using a fixed-bed adsorption system has not been investigated thoroughly. It is necessary to conduct this type of adsorption to judge the feasibility of applying these promising adsorbents on a pilot scale.

4) Large-scale production of an adsorbent is determined by cost factor to make wastewater treatment more economical. Therefore, the economic feasibility of applying graphene oxide nanocomposites in removing contaminants from the environment should be analyzed.

6) The current study is limited to the removal of heavy metal ions, while with the exceptional physical and chemical properties of graphene oxide nanocomposites, the applications should be extended to the adsorption towards other contaminants such as

fluorides, sulfur compounds, oils, antibiotics in conjunction with the in-situ detection of contaminants.

7) To date, most studies are restricted to adsorption; while future research should address the need of coupling adsorption-photocatalytic degradation via the incorporation of photo-catalytic materials such as MOFs in order to further enhance the removal efficiency.

8) The separation performance of the synthetic nanocomposites could be further improved by introducing magnetic nanoparticles on the surface of graphene oxide nanosheets.

References

1. Geissen, V., et al., *Emerging pollutants in the environment: a challenge for water resource management.* International soil and water conservation research, 2015. **3**(1): p. 57-65.
2. Lande, E., *Heavy metal pollution in Trondheimsfjorden, Norway, and the recorded effects on the fauna and flora.* Environmental Pollution (1970), 1977. **12**(3): p. 187-198.
3. Basha, C.A., et al., *Heavy metal removal from copper smelting effluent using electrochemical cylindrical flow reactor.* Journal of Hazardous Materials, 2008. **152**(1): p. 71-78.
4. Chen, Q., et al., *Comparison of heavy metal removals from aqueous solutions by chemical precipitation and characteristics of precipitates.* Journal of Water Process Engineering, 2018. **26**: p. 289-300.
5. Borbély, G. and E. Nagy, *Removal of zinc and nickel ions by complexation–membrane filtration process from industrial wastewater.* Desalination, 2009. **240**(1-3): p. 218-226.
6. de los Ríos, A.P., et al., *Removal of metal ions from aqueous solutions by extraction with ionic liquids.* Journal of Chemical & Engineering Data, 2010. **55**(2): p. 605-608.
7. Kim, S.-J., et al., *Removal of heavy metal-cyanide complexes by ion exchange.* Korean Journal of Chemical Engineering, 2002. **19**(6): p. 1078-1084.

8. Yu, B., et al., *The removal of heavy metal from aqueous solutions by sawdust adsorption—removal of copper*. Journal of Hazardous Materials, 2000. **80**(1-3): p. 33-42.

9. Chowdhury, S. and R. Balasubramanian, *Recent advances in the use of graphene-family nanoadsorbents for removal of toxic pollutants from wastewater.* Advances in colloid and interface science, 2014. **204**: p. 35-56.

10. Shao, L., et al., *PVA/polyethyleneimine-functionalized graphene composites with optimized properties.* Materials & Design, 2016. **99**: p. 235-242.

11. Shaban, M., et al., *Investigation the adsorption properties of graphene oxide and polyaniline nano/micro structures for efficient removal of toxic Cr (VI) contaminants from aqueous solutions; kinetic and equilibrium studies.* Rendiconti Lincei. Scienze Fisiche e Naturali, 2018. **29**(1): p. 141-154.

12. Qi, Y., et al., *Natural polysaccharides-modified graphene oxide for adsorption of organic dyes from aqueous solutions.* Journal of colloid and interface science, 2017. **486**: p. 84-96.

13. Muñoz, E., et al., *Highly conducting carbon nanotube/polyethyleneimine composite fibers.* Advanced Materials, 2005. **17**(8): p. 1064-1067.

14. Nguyen, H., et al., *Evaluation of polyether-polyethyleneimine graft copolymers as gene transfer agents.* Gene therapy, 2000. **7**(2): p. 126-138.

15. Sanz, R., et al., *CO2 adsorption on branched polyethyleneimine-impregnated mesoporous silica SBA-15.* Applied Surface Science, 2010. **256**(17): p. 5323-5328.

16. Bao, S., et al., *PEI grafted amino-functionalized graphene oxide nanosheets for ultrafast and high selectivity removal of Cr (VI) from aqueous solutions by adsorption combined with reduction: Behaviors and mechanisms.* Chemical Engineering Journal, 2020. **399**: p. 125762.

17. Liu, H., et al., *Synthesis of polyethylenimine/graphene oxide for the adsorption of U (VI) from aqueous solution.* Applied Surface Science, 2019. **471**: p. 88-95.

18. Saad, D., *Development and application of functionalized polymeric materials for heavy metal ions recovery from industrial and mining wastewaters*. 2013, Citeseer.

19. Ahuja, S., et al., *Comprehensive water quality and purification*. 2014: Elsevier Amsterdam.

20. Schmidt, C.K., F.T. Lange, and H.-J. Brauch. *Assessing the impact of different redox conditions and residence times on the fate of organic micropollutants during riverbank filtration*. in *4th International Conference on Pharmaceuticals and Endocrine Disrupting Chemicals in Water*. 2004.

21. Bessa, A., et al., *Graphene oxide/polyethyleneimine aerogel for high-performance mercury sorption from natural waters.* Chemical Engineering Journal, 2020. **398**: p. 125587.

22. Wang, X., et al., *3D self-assembly polyethyleneimine modified graphene oxide hydrogel for the extraction of uranium from aqueous solution.* Applied Surface Science, 2017. **426**: p. 1063-1074.

23. Tadjenant, Y., et al., *Graphene oxide chemically reduced and functionalized with KOH-PEI for efficient Cr (VI) adsorption and reduction in acidic medium.* Chemosphere, 2020. **258**: p. 127316.

24. Gari, L., *Arabic treatises on environmental pollution up to the end of the thirteenth century.* Environment and History, 2002: p. 475-488.

25. Rai, P.K., *Particulate matter and its size fractionation.* Biomagnetic Monitoring of Particulate Matter, 2016. **1**: p. 1-13.

26. Hinrichsen, D. and H. Tacio, *The coming freshwater crisis is already here.* The linkages between population and water. Washington, DC: Woodrow Wilson International Center for Scholars, 2002: p. 1-26.

27. *https://www.who.int/en/*.

28. Davis, M.L. and D.A. Cornwell, *Introduction to environmental engineering*. 2008: McGraw-Hill.

29. Wu, Y. and J. Chen, *Investigating the effects of point source and nonpoint source pollution on the water quality of the East River (Dongjiang) in South China.* Ecological indicators, 2013. **32**: p. 294-304.

30. Zhang, X., et al., *Graphene oxide caged in cellulose microbeads for removal of malachite green dye from aqueous solution.* Journal of colloid and interface science, 2015. **437**: p. 277-282.

31. Azizullah, A., et al., *Water pollution in Pakistan and its impact on public health—a review.* Environment international, 2011. **37**(2): p. 479-497.

32. Revenga, C. and G. Mock, *Dirty water: Pollution problems persist.* World Resources Institute, 2000.

33. Андрусишина, И., И. Голуб, and З. Малецкий, *HOW DANGEROUS LEAD IN DRINKING WATER?(LITERATURE REVIEW).* WATER AND WATER PURIFICATION TECHNOLOGIES. SCIENTIFIC AND TECHNICAL NEWS, 2016. **19**(2): p. 40-50.

34. Mahurpawar, M., *Effects of heavy metals on human health.* International Journal of Research-Granthaalayah, 2015. **3**(9SE): p. 1-7.

35. Costa, M., *Potential hazards of hexavalent chromate in our drinking water.* Toxicology and applied pharmacology, 2003. **188**(1): p. 1-5.

36. Chen, J., et al., *The spatiotemporal structure of twentieth-century climate variations in observations and reanalyses. Part I: Long-term trend.* Journal of Climate, 2008. **21**(11): p. 2611-2633.

37. *https://www.epa.gov/sdwa*.

38. Baccar Ep Yangui, R., M. Sarrà i Adroguer, and P. Blánquez Cano, *Removal of water pollutants by adsorption on activated carbon prepared from olive-waste cakes and by biological treatment using ligninolytic fungi*. 2014: Universitat Autònoma de Barcelona.

39. El-Gendy, A., et al., *Carbon-based materials (CBMS) for determination and remediation of antimicrobials in different substrates: Wastewater and infant foods as examples.* Carbon-Based Material for Environmental Protection and Remediation; Bartoli, M., Frediani, M., Rosi, L., Eds, 2020: p. 103-122.

40. Hendricks, D., *Fundamentals of water treatment unit processes: physical, chemical, and biological*. 2016: Crc Press.

41. Cheremisinoff, N.P., *Handbook of water and wastewater treatment technologies*. 2001: Butterworth-Heinemann.

42. Dombrowski, E.-M., U. Wiesmann, and I. Choi, *Fundamental of biological wastewater treatment*. 2014: Weinheim: Wiley-VCH Verlag GmbH & Co. KGaA p.

43. Woodard, F., *Industrial waste treatment handbook*. 2001: Elsevier.

44. Rodriguez-Freire, L., J. Gonzalez-Estrella, and G. Li. *Technologies for fractionation of wastewater and resource recovery*. in *Wastewater Treatment Residues as Resources for Biorefinery Products and Biofuels*. 2020.

45. Khulbe, K. and T. Matsuura, *Removal of heavy metals and pollutants by membrane adsorption techniques.* Applied water science, 2018. **8**(1): p. 1-30.

46. Pang, F.M., et al., *Removal of lead, zinc and iron by coagulation–flocculation.* Journal of the Taiwan Institute of Chemical Engineers, 2011. **42**(5): p. 809-815.

47. Bashir, A., et al., *Removal of heavy metal ions from aqueous system by ion-exchange and biosorption methods.* Environmental Chemistry Letters, 2019. **17**(2): p. 729-754.

48. Lakherwal, D., *Adsorption of heavy metals: a review*. International journal of environmental research and development, 2014. **4**(1): p. 41-48.

49. Gupta, V.K., et al., *Low-cost adsorbents: growing approach to wastewater treatment—a review.* Critical reviews in environmental science and technology, 2009. **39**(10): p. 783-842.

50. Ramaswamy, S., H.-J. Huang, and B.V. Ramarao, *Separation and purification technologies in biorefineries*. 2013: John Wiley & Sons Incorporated.

51. Anfar, Z., et al., *Recent trends on numerical investigations of response surface methodology for pollutants adsorption onto activated carbon materials: A review.* Critical Reviews in Environmental Science and Technology, 2020. **50**(10): p. 1043-1084.

52. Dąbrowski, A., *Adsorption—from theory to practice.* Advances in colloid and interface science, 2001. **93**(1-3): p. 135-224.

53. Nimibofa, A., et al., *Fullerenes: synthesis and applications.* J Mater Sci, 2018. **7**: p. 22-33.

54. Baby, R., B. Saifullah, and M.Z. Hussein, *Carbon nanomaterials for the treatment of heavy metal-contaminated water and environmental remediation.* Nanoscale research letters, 2019. **14**(1): p. 1-17.

55. Taamneh, Y. and S. Sharadqah, *The removal of heavy metals from aqueous solution using natural Jordanian zeolite.* Applied Water Science, 2017. **7**(4): p. 2021-2028.

56. Kausar, A., et al., *Dyes adsorption using clay and modified clay: a review.* Journal of Molecular Liquids, 2018. **256**: p. 395-407.

57. Zhao, K., et al., *Hooped amino-group chains in porous organic polymers for enhancing heavy metal ion removal.* ACS applied materials & interfaces, 2019. **11**(47): p. 44751-44757.

58. Rashed, M.N., *Adsorption technique for the removal of organic pollutants from water and wastewater.* Organic pollutants-monitoring, risk and treatment, 2013. **7**: p. 167-194.

59. Loh, K.P., et al., *The chemistry of graphene.* Journal of Materials Chemistry, 2010. **20**(12): p. 2277-2289.

60. Novoselov, K., et al., *Electric field in atomically thin carbon films.* Science. **2004**: p. 306.

61. Yousefi, N., et al., *Environmental performance of graphene-based 3D macrostructures.* Nature nanotechnology, 2019. **14**(2): p. 107-119.

62. Kayhan, E., *Graphene: Synthesis, Characterization, Properties and Functional Behavior as Catalyst Support and Gas Sensor.* 2013.

63. Yu, H., et al., *High-efficient synthesis of graphene oxide based on improved hummers method.* Scientific reports, 2016. **6**: p. 36143.

64. Dimiev, A., et al., *Pristine graphite oxide.* Journal of the American Chemical Society, 2012. **134**(5): p. 2815-2822.

65. Wang, J., Z. Chen, and B. Chen, *Adsorption of polycyclic aromatic hydrocarbons by graphene and graphene oxide nanosheets.* Environmental science & technology, 2014. **48**(9): p. 4817-4825.

66. Dreyer, D.R., A.D. Todd, and C.W. Bielawski, *Harnessing the chemistry of graphene oxide.* Chemical Society Reviews, 2014. **43**(15): p. 5288-5301.

67. Liu, Z.-B., et al., *Porphyrin and fullerene covalently functionalized graphene hybrid materials with large nonlinear optical properties.* The Journal of Physical Chemistry B, 2009. **113**(29): p. 9681-9686.

68. Gao, W., *The chemistry of graphene oxide*, in *Graphene oxide*. 2015, Springer. p. 61-95.

69. Bai, H., et al., *On the gelation of graphene oxide.* The Journal of Physical Chemistry C, 2011. **115**(13): p. 5545-5551.

70. Lee, J., et al., *Investigation of the mechanism of chromium removal in (3-aminopropyl) trimethoxysilane functionalized mesoporous silica.* Scientific reports, 2018. **8**(1): p. 1-11.

71. Geng, J., et al., *Polyethyleneimine cross-linked graphene oxide for removing hazardous hexavalent chromium: Adsorption performance and mechanism.* Chemical Engineering Journal, 2019. **361**: p. 1497-1510.

72. Huang, Z.-W., et al., *Simultaneous elimination of cationic uranium (VI) and anionic rhenium (VII) by graphene oxide–poly (ethyleneimine) macrostructures: a batch, XPS, EXAFS, and DFT combined study.* Environmental Science: Nano, 2018. **5**(9): p. 2077-2087.

73. Zhao, Q., X. Zhu, and B. Chen, *Stable graphene oxide/poly (ethyleneimine) 3D aerogel with tunable surface charge for high performance selective removal of ionic dyes from water.* Chemical Engineering Journal, 2018. **334**: p. 1119-1127.

74. Xi, J., et al., *Anchoring DTPA grafted PEI onto carboxylated graphene oxide to effectively remove both heavy metal ions and dyes from wastewater with robust stability.* Journal of Materials Science, 2021: p. 1-17.

75. Wang, L., et al., *Graphene oxide/ferroferric oxide/polyethylenimine nanocomposites for Congo red adsorption from water.* Environmental technology, 2017. **38**(8): p. 996-1004.

76. Schniepp, H.C., et al., *Functionalized single graphene sheets derived from splitting graphite oxide.* The Journal of Physical Chemistry B, 2006. **110**(17): p. 8535-8539.

77. Allen, M.J., V.C. Tung, and R.B. Kaner, *Honeycomb carbon: a review of graphene.* Chemical reviews, 2010. **110**(1): p. 132-145.

78. Miraftab, R., et al., *An advanced approach for fabricating a reduced graphene oxide-AZO dye/polyurethane composite with enhanced ultraviolet (UV) shielding properties: Experimental and first-principles QM modeling.* Chemical Engineering Journal, 2017. **321**: p. 159-174.

79. Kumar JR, N., et al., *A potential application of polyethyleneimine-reduced graphene oxide nanocomposite sensing film coated on interdigitated electrode prepared from copper-clad for carbon dioxide detection.* Materials Research Innovations, 2021. **25**(6): p. 363-371.

80. Langmuir, I., *The adsorption of gases on plane surfaces of glass, mica and platinum.* Journal of the American Chemical society, 1918. **40**(9): p. 1361-1403.

81. He, Y., et al., *One-step fabrication of PEI-modified GO particles for CO 2 capture.* Applied Physics A, 2019. **125**(3): p. 160.

82. Miraftab, R., et al., *Complementary experimental and quantum mechanics approaches for exploring the mechanical characteristics of epoxy composites loaded with graphene oxide-polyaniline nanofibers.* Journal of industrial and engineering chemistry, 2017. **53**: p. 348-359.

83. Ramezanzadeh, M., et al., *Corrosion resistance of epoxy coating on mild steel through polyamidoamine dendrimer-covalently functionalized graphene oxide*

nanosheets. Journal of Industrial and Engineering Chemistry, 2020. **82**: p. 290-302.

84. Mei, Q., et al., *Highly efficient photoluminescent graphene oxide with tunable surface properties.* Chemical communications, 2010. **46**(39): p. 7319-7321.

85. Liu, H., et al., *In situ synthesis of the reduced graphene oxide–polyethyleneimine composite and its gas barrier properties.* Journal of materials chemistry a, 2013. **1**(11): p. 3739-3746.

86. Balan, C., I. Volf, and D. Bilba, *Chromium (VI) removal from aqueous solutions by purolite base anion-exchange resins with gel structure.* Chemical Industry and Chemical Engineering Quarterly/CICEQ, 2013. **19**(4): p. 615-628.

87. Yang, B., et al., *The adsorption of Cu species onto pyrite surface and its effect on pyrite flotation.* Journal of Chemistry, 2016. **2016**.

88. Giraldo, L. and J. Moreno-Piraján, *Pb2+ adsorption from aqueous solutions on activated carbons obtained from lignocellulosic residues.* Brazilian Journal of Chemical Engineering, 2008. **25**(1): p. 143-151.

89. Zhou, G., et al., *Sponge-like polysiloxane-graphene oxide gel as a highly efficient and renewable adsorbent for lead and cadmium metals removal from wastewater.* Chemical Engineering Journal, 2015. **280**: p. 275-282.

90. Kumar, N., E. Fosso-Kankeu, and S.S. Ray, *Achieving controllable MoS2 nanostructures with increased interlayer spacing for efficient removal of Pb (II) from aquatic systems.* ACS applied materials & interfaces, 2019. **11**(21): p. 19141-19155.

91. Kong, Q., et al., *Fabrication of terminal amino hyperbranched polymer modified graphene oxide and its prominent adsorption performance towards Cr (VI).* Journal of hazardous materials, 2019. **363**: p. 161-169.

92. Xue, F., et al., *Structural design of a cellulose-based solid amine adsorbent for the complete removal and colorimetric detection of Cr (VI).* Langmuir, 2019. **35**(39): p. 12636-12646.

93. Zhao, L., et al., *Application of carboxymethyl cellulose–stabilized sulfidated nano zerovalent iron for removal of Cr (VI) in simulated groundwater.* Water, Air, & Soil Pollution, 2019. **230**(6): p. 1-14.

94. Feng, N., X. Guo, and S. Liang, *Adsorption study of copper (II) by chemically modified orange peel.* Journal of Hazardous Materials, 2009. **164**(2-3): p. 1286-1292.

95. El-Ashtoukhy, E.-S., N.K. Amin, and O. Abdelwahab, *Removal of lead (II) and copper (II) from aqueous solution using pomegranate peel as a new adsorbent.* Desalination, 2008. **223**(1-3): p. 162-173.

96. Kumar, P.S., et al., *Thermodynamic and kinetic studies of cadmium adsorption from aqueous solution onto rice husk.* Brazilian Journal of Chemical Engineering, 2010. **27**: p. 347-355.

Curriculum Vitae

Candidate's full name: Roshanak Miraftab

Universities attended :University of New Brunswick, 2019 – 2021

M.ScE Candidate, Department of Chemical Engineering

Amirkabir University of Technology, Iran, 2008 – 2013

Bachelor of Science (B.Sc.), Department of Polymer engineering

Publications:

Miraftab, Roshanak, and Xiao. Huining. "Feasibility and potential of graphene and its hybrids with cellulose as drug carriers: a commentary." *Journal of Bioresources and Bioproducts* 4.4 (2019): 200-201.

X. Hou, R. Miraftab, H. Xiao et al. "Redox-and Enzyme-Responsive Macrospheres Gatekept by Polysaccharides for Controlled Release of Agrochemicals." *Journal of Agricultural and Food Chemistry* , 69, 38(2021): 11163–11170.

Miraftab, Roshanak, et al. "Complementary experimental and quantum mechanics approaches for exploring the mechanical characteristics of epoxy composites loaded with graphene oxide-polyaniline nanofibers." *Journal of industrial and engineering chemistry* 53 (2017): 348-359.

Ramezanzadeh, Bahram, et al. "Impact of size-controlled p-phenylenediamine (PPDA)-functionalized graphene oxide nanosheets on the GO-PPDA/Epoxy anti-corrosion, interfacial interactions and mechanical properties enhancement: Experimental and quantum mechanics investigations." *Chemical Engineering Journal* 335 (2018): 737-755.

Miraftab, R., et al. "An advanced approach for fabricating a reduced graphene oxide-AZO dye/polyurethane composite with enhanced ultraviolet (UV) shielding properties: Experimental and first-principles QM modeling." *Chemical Engineering Journal* 321 (2017): 159-174.

Work Experience:

Research assistant, Lucent BioSciences, Inc. , Canada, (May. 2021 – August 2021)